Satellite Application Facility on support to operational Hydrology and water Management (H-SAF)

Evaluation on accuracy of precipitation data

Final Report on the Visiting Scientist Activities

Marco Petracca

13/12/2011

Acknowledgments

This work was made possible by the support and assistance of a number of people whom I would like to personally thank.

It is a great pleasure to thank my tutors *Francesco Zauli*, *Federico Porcù* and *Emanuele Vuerich* for their determination and for the impressive volume of work they have done to support me in any possible aspect.

My full respect goes to the H-SAF Project Manager, in the person of *Luigi De Leonibus* for the interest constantly showed in the project.

A special thank goes to the H-SAF Science Manager, *Paolo Rosci* not only for his kindness but also for his technical support.

I would also like to thank *Antonio Vocino*, *Daniele Biron*, *Davide Melfi*, *Massimiliano Sist* and *Luigi Spadacenta* for their precious help and more important for their friendly and professional attitude.

It has been a true pleasure to work in collaboration with the Italian Meteorological Service of the Airforce, for the resources they provided and for their priceless hospitality.

Marco Petracca

CONTENTS

1 INTRODUCTION

The HSAF is a consortium to retrieve observation dedicated to hydrology monitoring. In particular the consortium produces: estimate of instantaneous precipitation from SSM I/S and AMSU/MHS instruments and accumulated precipitation with a IR/MW blending technique.

During the Development Phase (DP) of H-SAF a suite to evaluate the accuracy of precipitation maps retrieved from satellite data has been implemented. This service is very important to ingest the observation in a numerical model or in a decisional cycle. Two different methodologies has been implemented to evaluate the performance of products: the first is the validation of retrieved values respect the a field built using in situ parameter observations considered as the "*truth*"; the second one is based on the evaluation of the output of an hydrological model. The present study aims to investigate some aspects of the first method. In the H-SAF context instantaneous and accumulated precipitation have been usually evaluated respect to radar and rain gauge (RG) data. Radar and RG derived fields have been assumed as the "truth" and no error has been considered. The experience and the literature show that this assumption is not correct (Graves, Valdès, Shen and North (1993), Llasat, Rigo, Ceperuelo and Barrera (2005), Lanza, Vuerich and Gnecco (2010)). It is necessary to understand that the ground data are not truth but they are the best reference data. This study wants clarify about the error structure of precipitation field retrieved from radars and RG evaluating the limits of accuracy requirements proposed during the DP.

The HSAF Validation Group (VG) calculated the error in rainfall estimation from satellite considering as reference rain measured by RG at ground. The result of this validation activity indicates the difference between the satellite and the ground measurement; it is the Root Mean Square Difference (RMSD) of satellite vs. reference that should be:

$$RMSD = \sqrt{RMSE_{sat} + RMSE_{ground} + RMSE_{comparison}}$$

where:

- $RMSE_{sat}$ is the error due to satellite rainfall estimation that should be final result of the validation activity. It contains some errors intrinsic to the product as geolocation, time-matching and parallax errors. $RMSE_{sat}$ can be obtained by the inverse formula, if other terms in equation are known;
- $RMSE_{ground}$ is the error due to the RG at ground (from the literature it is approximately about 50-100% for instantaneous precipitation and about 25-50% for cumulated precipitation).
- $RMSE_{comparison}$ is the error due to the method used to compare satellite data with reference ground data and it is due mainly to the upscaling/downscaling and interpolation process.

The Visiting Scientist's work consists to quantify $RMSE_{comparison}$ and $RMSE_{ground}$ to evaluate $RMSE_{sat}$, and therefore the accuracy of satellite rainfall estimation.

This report is structured as follows:

- The *Estimation of RMSEcomparison chapter* deals with comparison errors and it is divided in:
  a) *Dataset section* where the data used are presented;
  b) *Methodology section* deals with approach used to estimate comparison errors;
  c) *Analysis and Results section* where results and comments are summarized;
- The *Estimation of RMSEground chapter* deals with instrumental errors;
- The *Comparison of interpolation methods chapter* describes the comparison between two of the most widely used interpolation methods applied by VG to different spatial density RG data;
- The *Continuous precipitation field retrieved from ground data chapter* describes a prototype of a continuous precipitation field obtained from RG data and a NWP model;
- *Conclusions* summarizes the work and results obtained*;*

2 ESTIMATION OF RMSE$_{COMPARISON}$

In this section is explained the approach used for analysis of precipitation fields to estimate the comparison error between satellite and radars/RG. Data used in the study are here presented. Later, in the section 2.2 the methodology used for data analysis is explained and finally in section 2.3 the results obtained are displayed.

2.1 DATASET

This section shows data used in this work. Instantaneous rain radar data on a regular grid of 1200 x 1200 pixels with a spatial resolution of 1 x 1 Km and temporal resolution of 15 minutes are used because represent a true precipitation field useful to evaluate the technique of downscaling used in H-SAF validation activity. These data represent the mosaic of radar data collected by the Italian national network and are provided by DPC.

Characteristics of Dataset	Value
Temporal Resolution	15 min.
Spatial Resolution	1 x 1 Km
Dimensions	1200 x 1200 pixels
Centered on	Italy
Events of	28 March 2011 (00:30 – 16:45); 8 and 22 November 2010 (00:15 – 23:00)
Total number of precipitation fields	248 instants (15 min/instant): 64 (March 2011); 184 (November 2010)

TAB. 2.1 – CHARACTERISTICS OF DATASET USED IN THIS WORK.

Fig. 2.1 shows a snapshot of the native precipitation field.

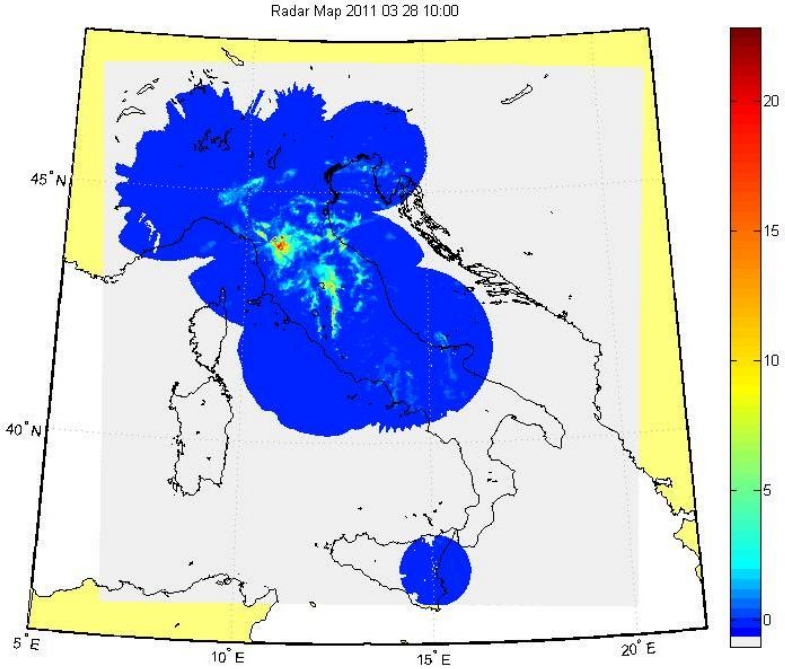

FIG. 2.1 – EXAMPLE OF AN INSTANT OF THE NATIVE PRECIPITATION FIELD MAPPED ON ITALY.

2.2 METHODOLOGY

$RMSE_{comparison}$ refers to the limitations of the comparison method between satellite and RG data that, in spite of all efforts envisaged and implemented by the validation teams, has left residual errors difficult to be further reduced, but needing evaluation by in-depth investigation. This type of error is due mainly to the interpolation and upscaling/downscaling processes. These processes to make compatible the instrument resolution and the ground station representativeness have been applied, for instance by applying Gaussian filters, but the statistics of residual errors are not available; this problem affects radar to a minor extent than RG, that may explain why comparisons with radar finally are not worse than with RG.

To evaluate the performance of techniques of downscaling a short theoretical experiment has been implemented. An hypothetic perfect field has been assumed. The field has been reduced, some points are been removed in regular and randomly manner to evaluate the capability of some techniques to reproduce the original fields.

To built the hypothetic field has been used the radar maps.

For every instant of native precipitation field the maximum of precipitation has been found and a subarea of 111 x 111 pixels centered on it was extracted (see Fig. 2.2). In total 64 instants for the event of 28 march 2011 (from 00:30 to 16:45) are extracted.

To simulate the spatial loss of information by gauges different sampling are been done. These data are sampled at different **regular** grid unit (g. u.) spacing (by step 2, 3 and 4 g. u., see Fig. 2.3) to obtain new data at different spatial density. So, for regular sampling by step 2 are obtained a total of 3136 grid points for each instant: 56 values (out of 111) along X-axes and 56 (out of 111) along Y-axes. For step 3 are obtained 37 grid points (out of 111) along X-axes and 37 along Y-axes for a total of 1369 grid points. At the same mode, for step 4 are obtained 28 x 28 = 784 total grid points (see Tab. 2.2).

Regular Step	Original field: X and Y size [pixel]	Original field: total number of pixels	Sampled field: X and Y size [pixel]	Sampled field: total number of pixels
2	111, 111	12321 (=111x111)	56, 56	3136 (=56x56)
3	111, 111	12321 (=111x111)	37, 37	1369 (=37x37)
4	111, 111	12321 (=111x111)	28, 28	784 (=28x28)

TAB. 2.2 – NUMBER OF GRID POINTS (OR PIXELS) FOR REGULARLY SAMPLED DATA GRID.

So, for each instant and step, a fixed number of grid points extracted by original field are obtained. Then, this grid points are been interpolated to rebuilt the new field of same dimensions of the original one. This interpolation process is made through different algorithms that are: Barnes, IDS, Kriging and NN (as shows in Fig. 2.4).

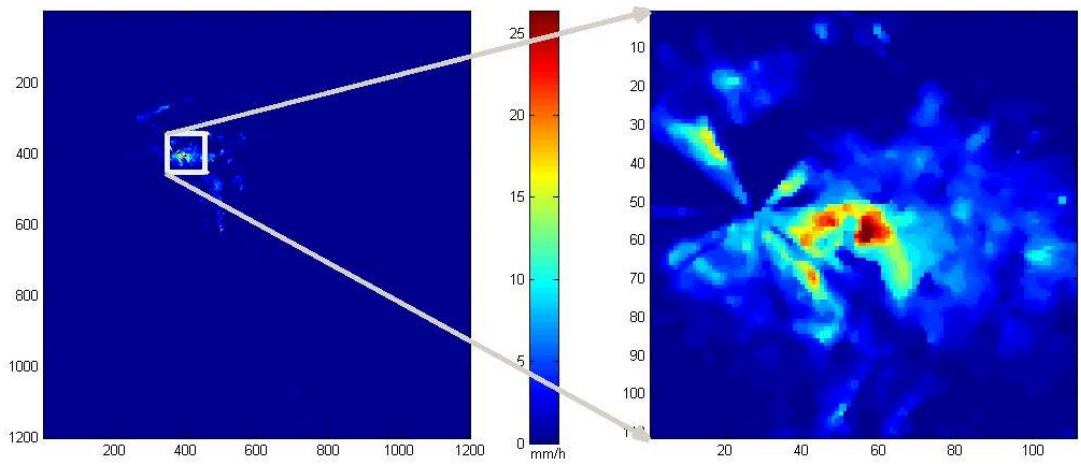

FIG. 2.2 – ON THE LEFT: AN INSTANT OF THE NATIVE PRECIPITATION FIELD (1200 X 1200 PIXELS). ON THE RIGHT: THE ORIGINAL PRECIPITATION FIELD (111 X 111 PIXELS) EXTRACTED AND CENTERED ON THE MAXIMUM OF PRECIPITATION.

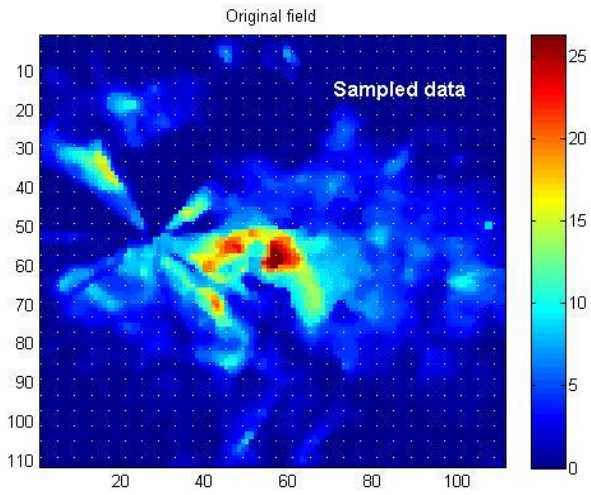

FIG. 2.3 ORIGINAL FIELD REGULARLY SAMPLED DATA BY STEP 4 GRID UNIT. SAMPLED DATA ARE INDICATED BY LITTLE DOTS.

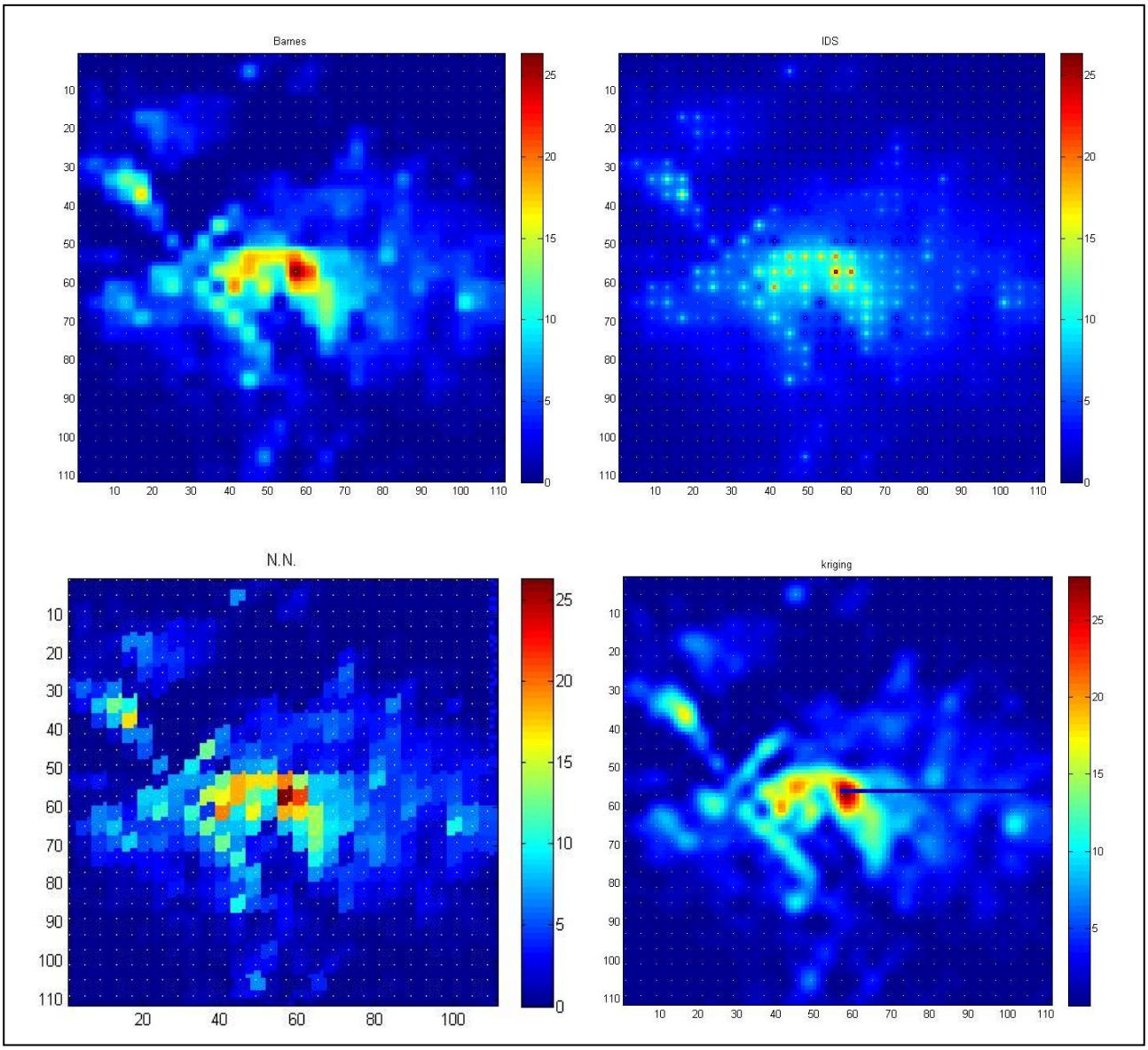

FIG. 2.4 - EXAMPLES OF INTERPOLATIONS REGULARLY SAMPLED DATA BY STEP 4. SAMPLED DATA ARE INDICATED BY LITTLE DOTS.

Then, for each instant, some statistics are calculated as: the minimum, maximum, average, standard deviation (STD) and percentage of zeros for the original data and the minimum, maximum, average, STD, accuracy, RMSE % and bias for the interpolated data. The formulas used are:

$$Standard\ Deviation\ (STD) = \sqrt{\frac{1}{N}\sum_{i=1}^{N}(X_i - \bar{X})^2}$$

with $\bar{X} = \sum_{i=1}^{N} X_i/N$ is the mean value of X_i elements;

$$accuracy = \frac{hits}{total}$$

where *hits* are the number of grid points equal in the original field and in the interpolated field;

$$Root\ Mean\ Square\ Error\ (RMSE)\% = \sqrt{\frac{1}{N}\sum_{i=1}^{N}\frac{(sat_i - true_i)^2}{true_i{}^2}} * 100\%$$

where sat_i are the validating data, (as interpolated data) and $true_i$ are the references (as original data); N is the total number of pairs data in which the *true* values are greater than 0 [mm/h].

Finally, the mean value of RMSE % with corresponding STD mean value is calculated for interpolation of a regular data grid sampled at different steps and the results are shown and analyzed in the section 2.3.1.

To simulate a network-gauge a random sampling has been done. So, the original fields were sampled at different **irregular** step of g. u. This sampling is made maintaining constant the total number of grid points sampled for each step (as shows in Tab. 2.2) to compare the results. So, for step 2 are randomly chosen 3136 grid points, for step 3 are randomly chosen 1369 grid points and for step 4 are randomly chosen 784 grid points (see Fig. 2.5). The positions of grid points randomly chosen for that step are maintained constant for all instants and for all interpolation methods to have same sampled data. Then statistical analysis are made and the results are shown and analyzed in the section 2.3.2.

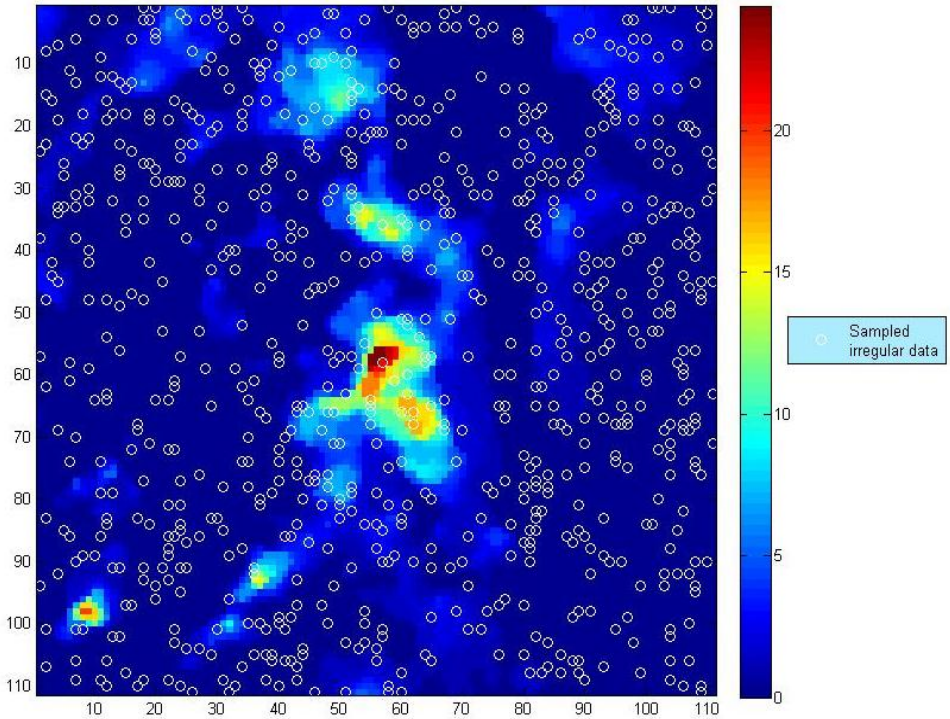

FIG. 2.5 – EXAMPLE OF AN ORIGINAL FIELD IRREGULARLY SAMPLED.

Assuming a different morphology of cumulated and instantaneous precipitation, the experiment has been performed also on cumulated fields. Then, **hourly precipitation** was analyzed at different **irregular** steps of grid. For each hour of data (4 instants x 15 minutes/instants) is calculated the hourly precipitation mean for each grid point of the native field. Original field (of dimensions 111 x 111 pixels) centered on the maximum value of hourly mean precipitation was extracted (as shows in Fig. 2.6). So, 14 hourly precipitation data are obtained for the event of the 28 march 2011. Then, this data are irregularly sampled (as above explained) and statically analyzed (see section 2.3.3).

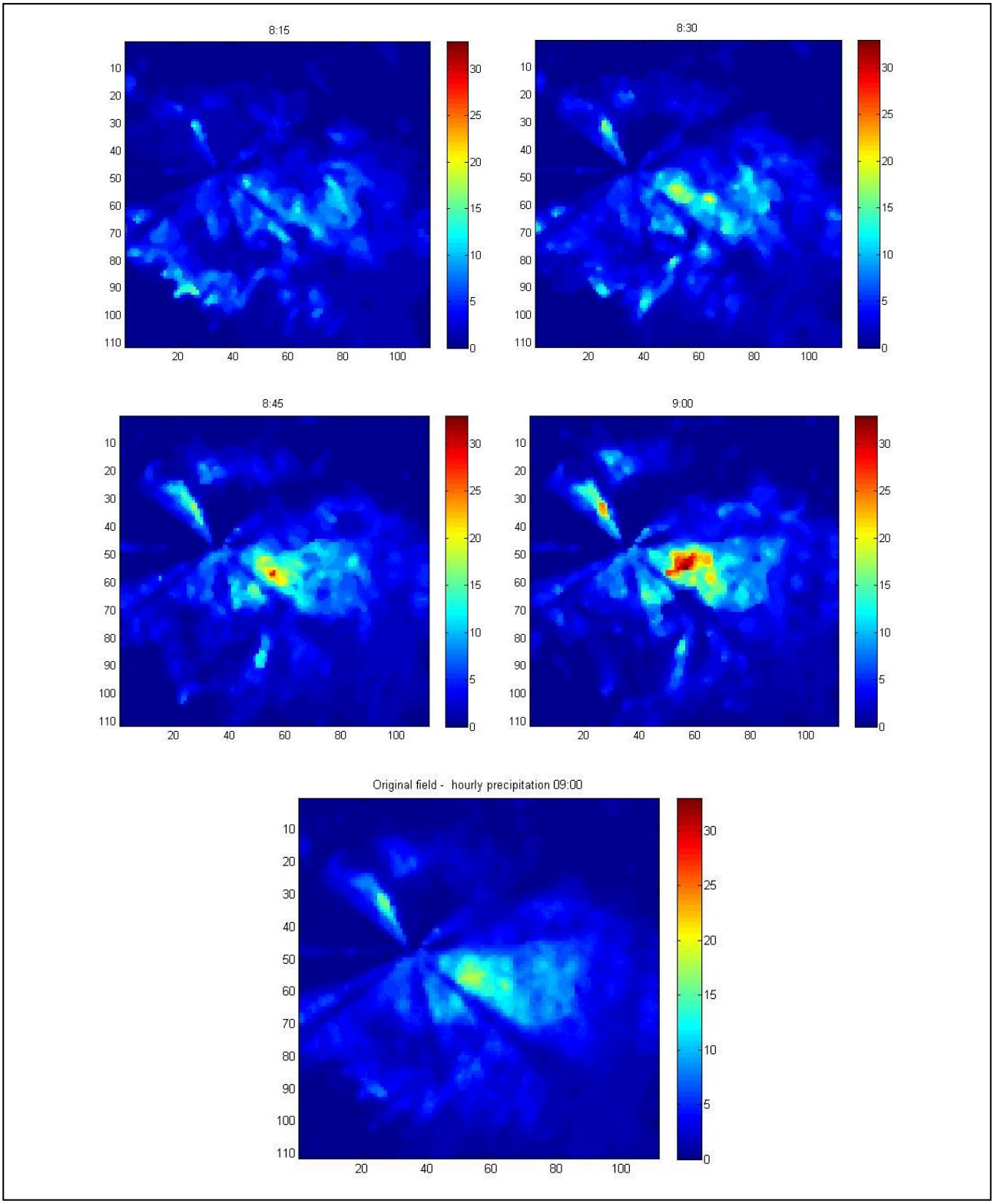

FIG. 2.6 - HOURLY PRECIPITATION. THE PICTURE BELOW IS THE MEAN PRECIPITATION OF 9:00. IT IS COMPUTED BY PRECIPITATION DATA FROM 8:15 TO 9:00.

The validation work carried on with RG uses about 3000 instruments across the 6 Countries irregularly distributed over the ground. A key characteristics of such networks is the distance between each RG and the closest one, averaged over all the instruments

considered in the network and it is a measure of the RG density. Instruments number and density are summarized in Tab. 2.3. The gauges density ranges between 7 (for Bulgaria, where only 3 river basins are considered) to 27 km (for Turkey).

Country	Total number of gauges *	Average minimum distance (km)
Belgium	89**	11.2
Bulgaria	37***	7
Germany	1300	17
Italy	1800	9.5
Poland	330÷475	13.3
Turkey	193****	27

TAB. 2.3 - NUMBER AND DENSITY OF RAINGAUGES WITHIN H-SAF VALIDATION GROUP.

* the number of RG could vary from day to day due to operational efficiency within a maximum range of 10-15%.
** only in the Wallonia Region.
*** only in 3 river basins.
**** only covering the western part of Anatolia.

The average minimum distance between points irregularly sampled was calculated in grid unit as shown in Tab. 2.4.

Step (g.u.)	2	3	4	5	6	7
Average minimum distance (g.u.)	1.2	1.6	2.1	2.5	3.1	3.6
Step (g.u.)	**8**	**9**	**10**	**11**	**12**	**13**
Average minimum distance (g.u.)	4.1	4.4	4.8	5.2	5.8	6.5

TAB. 2.4 – AVERAGE MINIMUM DISTANCE COMPUTED FOR EVERY STEP IRREGULARLY SAMPLED IN GRID UNIT.

Assuming that in the validation work the grid has a regular step of 5 km the gauges density in grid unit ranges between $\frac{7}{5} = 1.4$ g.u. for Bulgaria (near step 2÷3) to $\frac{27}{5} = 5.4$ g.u. for Turkey (near step 11) as it shown in Tab. 2.5. So the last analysis is made up to 11 irregular steps for hourly precipitation data (see page 20).

Country	Average minimum distance (g.u)	Adjacent step
Belgium	11.2/5=**2.2**	4
Bulgaria	7 /5=**1.4**	2÷3
Germany	17 /5=**3.4**	7
Italy	9.5/5=**1.9**	4
Poland	13.3/5=**2.7**	5
Turkey	27 /5=**5.4**	11

TAB. 2.5 – ADJACENT STEP FOR EVERY COUNTRY' S RG DENSITY ASSUMING A REGULAR GRID OF 5 KM.

2.3 ANALYSIS AND RESULTS

In this section results obtained in the VS's study are shown.

2.3.1 REGULARLY SAMPLED DATA GRID

To evaluate the existence of a dependence of capability to rebuilt the original field, the morphology of fields has been evaluated. The STD is a good parameter to evaluate the variance of intensity of maps. In Fig. 2.7 are plotted the values of STD of original field vs. RMSE% computed for each interpolation method.

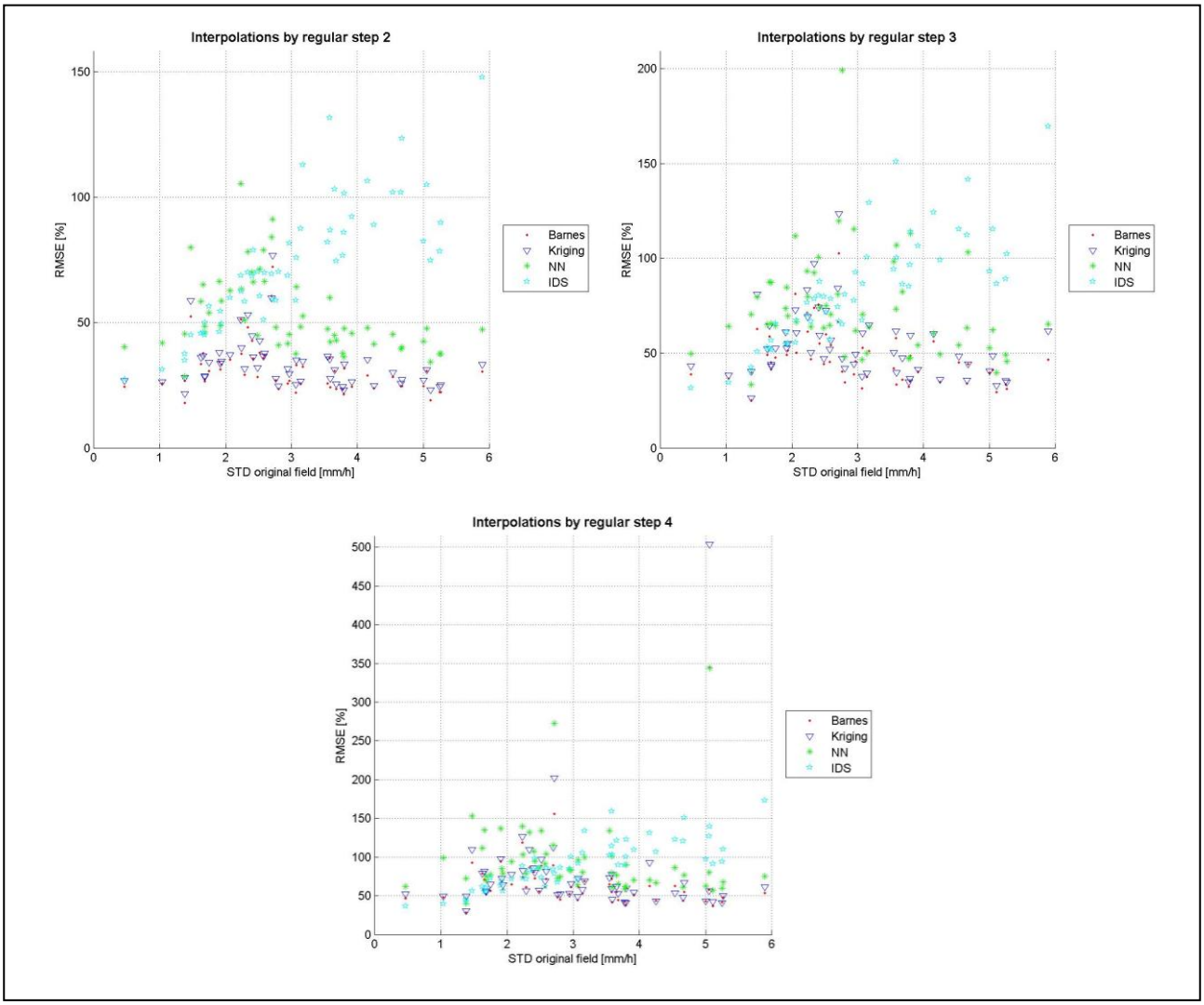

FIG. 2.7 – STD VS. RMSE% FOR REGULARLY SAMPLED PRECIPITATION DATA.

As shows in Fig. 2.7, RMSE% for all interpolation methods is enough constant at variation of STD of the original field (except for IDS). The mean values of RMSE % computed by the interpolation of regularly sampled data by step 2, 3 and 4 g.u. are summarized in Tab. 2.6:

Interpolation	RMSE mean [%] Step 2	Step 3	Step 4
Barnes	31.31 ± 10.18	47.82 ± 14.56	66.65 ± 43.38
Kriging	33.64 ± 10.33	53.55 ± 17.76	75.69 ± 64.32
NN	52.98 ± 15.75	73.66 ± 27.00	94.94 ± 48.67
IDS	73.51 ± 25.43	82.38 ± 28.91	90.76 ± 30.21

TAB. 2.6 – SUMMARY TABLE. RMSE MEAN VALUES % OBTAINED BY DIFFERENT INTERPOLATION METHODS AND STEPS FOR REGULARLY SAMPLED DATA GRID.

The mean STD value of 64 original fields is equal to 2.16 ± 1.18 [mm/h].

The Barnes interpolation method is the algorithm with the lower mean value of RMSE% and respective STD than other interpolation algorithms. Moreover, for all interpolations, values of RMSE % and respective STD increase with step.

In Fig. 2.8 is shown trend of RMSE% with the steps for regular sampling. All interpolation methods show trend of RMSE% values increase with the step with values between 31% (Barnes step 2) and 95% (NN step 4).

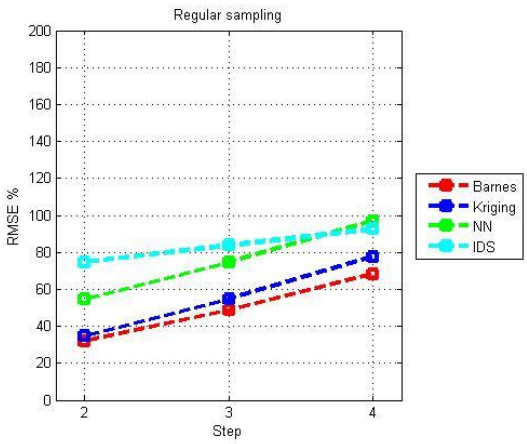

FIG. 2.8 – RMSE% COMPUTED FOR DIFFERENT REGULAR STEPS.

Barnes and Kriging methods have a similar trend, but Barnes shows best results.

2.3.2 IRREGULARLY SAMPLED DATA GRID

For every instant, has been found the maximum of precipitation and was extracted a subarea centered on maximum. This area, of 111x111 grid units is considered the original field. This original data are sampled in irregular mode. As in step 2, 56 values were chosen randomly; as in step 3, 37 values were chosen randomly and as in step 4, 28 values were chosen randomly (see Fig. 2.5).

From these random values the sampled field is created. Then, the interpolation processes are made through different algorithms: Barnes, Inverse Distance Squared (IDS), Kriging and Nearest Neighbor (NN) (as shows in Fig. 2.3).

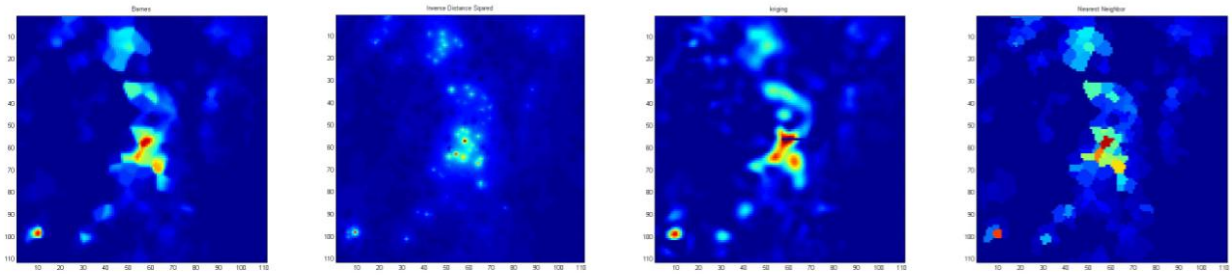

FIG. 2.3 – EXAMPLES OF INTERPOLATIONS BY IRREGULARLY SAMPLED DATA. FROM LEFT: BARNES, IDS, KRIGING AND NN INTERPOLATION METHOD.

For each instant some statistics are calculated: the minimum, maximum, average, STD and percentage of zeros for the original data and the minimum, maximum, average, STD, accuracy, RMSE % and bias for the interpolated data.

The mean values of RMSE % obtained by the interpolation of a irregularly sampled data by step 2, 3 and 4 grid units are follows:

Interpolation	RMSE mean [%]		
	Step 2	Step 3	Step 4
Barnes	44.02 ± 14.55	62.84 ± 17.67	91.76 ± 38.55
Kriging	56.80 ± 21.81	187.80 ± 61.25	151.09 ± 60.38
NN	56.89 ± 17.56	78.27 ± 21.82	114.90 ± 48.38
IDS	80.84 ± 27.22	91.77 ± 32.72	98.49 ± 35.42

TAB. 2.7 - SUMMARY TABLE. RMSE MEAN VALUES % OBTAINED BY DIFFERENT INTERPOLATION METHODS AND STEPS FOR IRREGULARLY SAMPLED DATA GRID.

The Barnes interpolation method is again the algorithm with the lower mean value of RMSE% and respective STD than other interpolation algorithms. Moreover, as noted above, values of RMSE % increases with step for all interpolations.

In Fig. 2.9 values of STD of original field vs. RMSE% computed for irregularly sampled data grid are plotted.

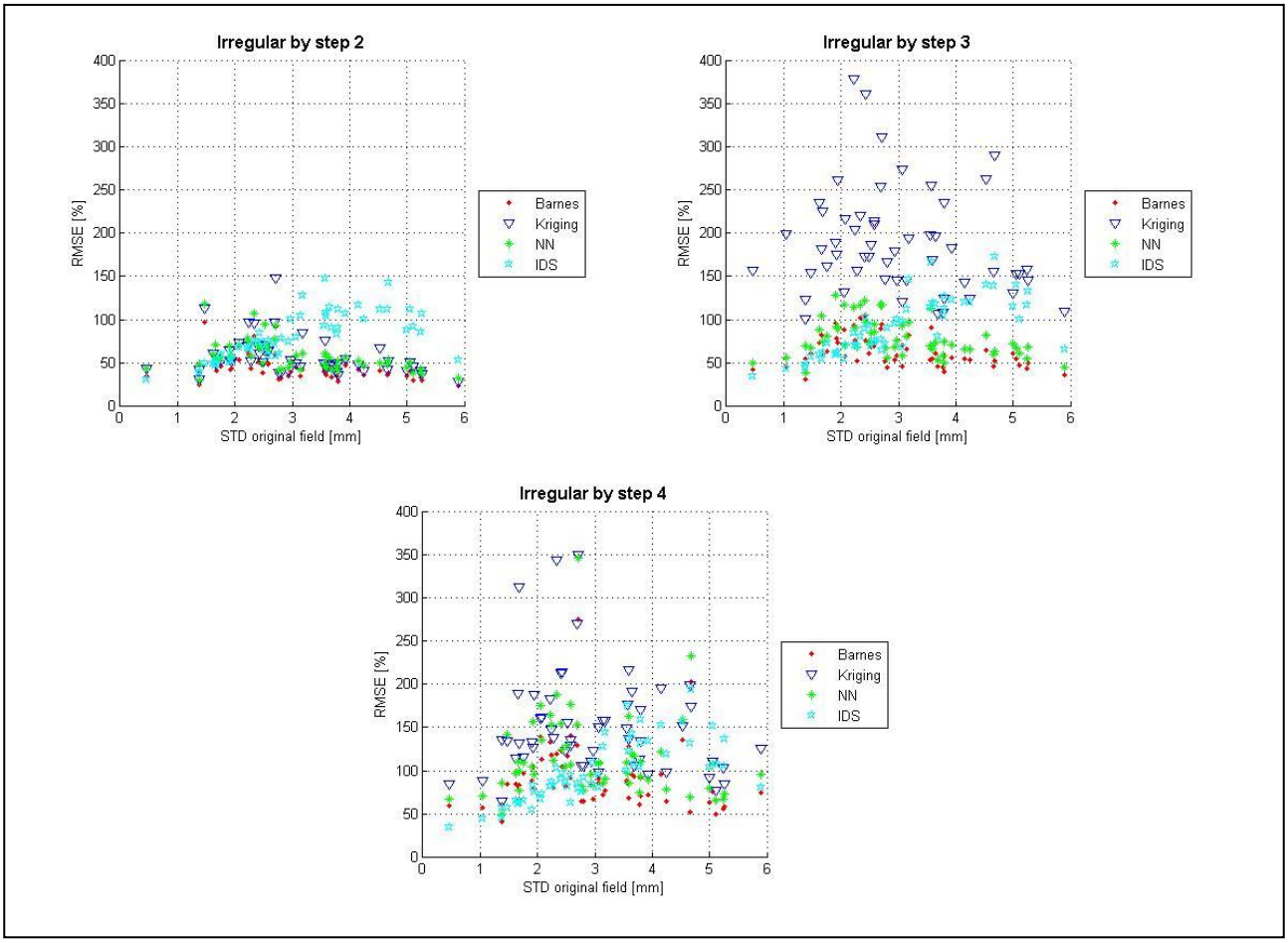

FIG. 2.9 - VS. RMSE% FOR INTERPOLATIONS IRREGULARLY SAMPLED PRECIPITATION DATA.

The Barnes and NN methods maintain constant low value with increasing of STD of original field.

In Fig. 2.10 is shown trend of RMSE% with the step for irregular sampling and for all interpolation methods. As above, all interpolation methods show trend of RMSE% values increase with the step (with values between 44% for Barnes at step 2 and 188% for Kriging at step 3). Kriging at step 3 shows an abnormal behaviour (as show in Fig. 2.9).

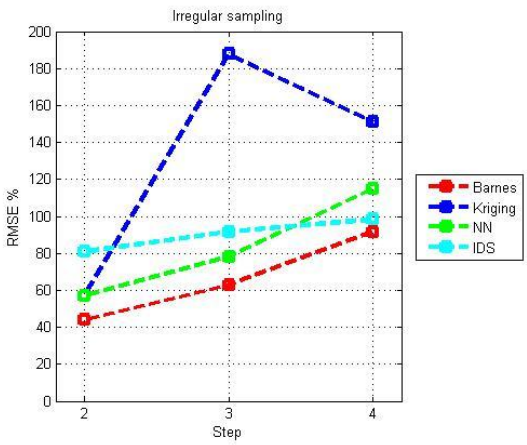

FIG. 2.10 – RMSE% COMPUTED FOR DIFFERENT IRREGULAR STEPS.

2.3.3 HOURLY PRECIPITATION DATA

Hourly precipitation data for the event of 28 March 2011 was analyzed. For each hour of data (4 instants x 15 minutes/instants) is calculated the mean precipitation point per point on a hour. So, 14 hourly precipitation data are. The results are summarized in Tab. 2.8.

Interpolation	RMSE mean [%]		
	Step 2	Step 3	Step 4
Barnes	24.99 ± 7.51	36.55 ± 10.29	52.46 ± 15.76
Kriging	30.50 ± 10.34	99.89 ± 53.78	81.56 ± 42.18
NN	32.30 ± 8.15	47.00 ± 12.73	66.11 ± 18.43
IDS	55.47 ± 17.66	66.45 ± 20.82	74.53 ± 28.94

TAB. 2.8 - RMSE MEAN VALUES % OBTAINED BY DIFFERENT INTERPOLATION METHODS AND STEPS FOR HOURLY IRREGULARLY SAMPLED DATA GRID.

The mean STD value of 14 original fields is equal to 2.05 ± 0.99 [mm/h].

The principal effect of the hourly precipitation's analysis is the decreasing of the STD values of the original fields due to the high temporal-spatial variability of precipitation. So, the mean RMSE% values computed for hourly precipitation data are smaller than instantaneous data of around 50% .

In Fig. 2.11 is shown trend of RMSE% with the step for irregular sampling of hourly mean precipitation. All interpolation methods show trend of RMSE% values increase with the step with values between 25% (barnes step 2) and 100% (Kriging step 3). For irregular sampling of hourly mean precipitation the RMSE% values are less than other previous sampling. The Barnes method shows smaller values of RMSE%.

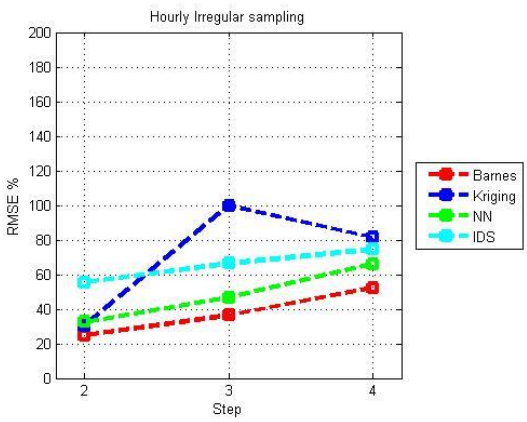

FIG. 2.11 – RMSE% COMPUTED FOR DIFFERENT STEPS.

In Fig. 2.12 there are graphics of STD vs. RMSE% obtained for irregularly sampled hourly precipitation data. In this case, statistic is low because the data analyzed are only a few hours.

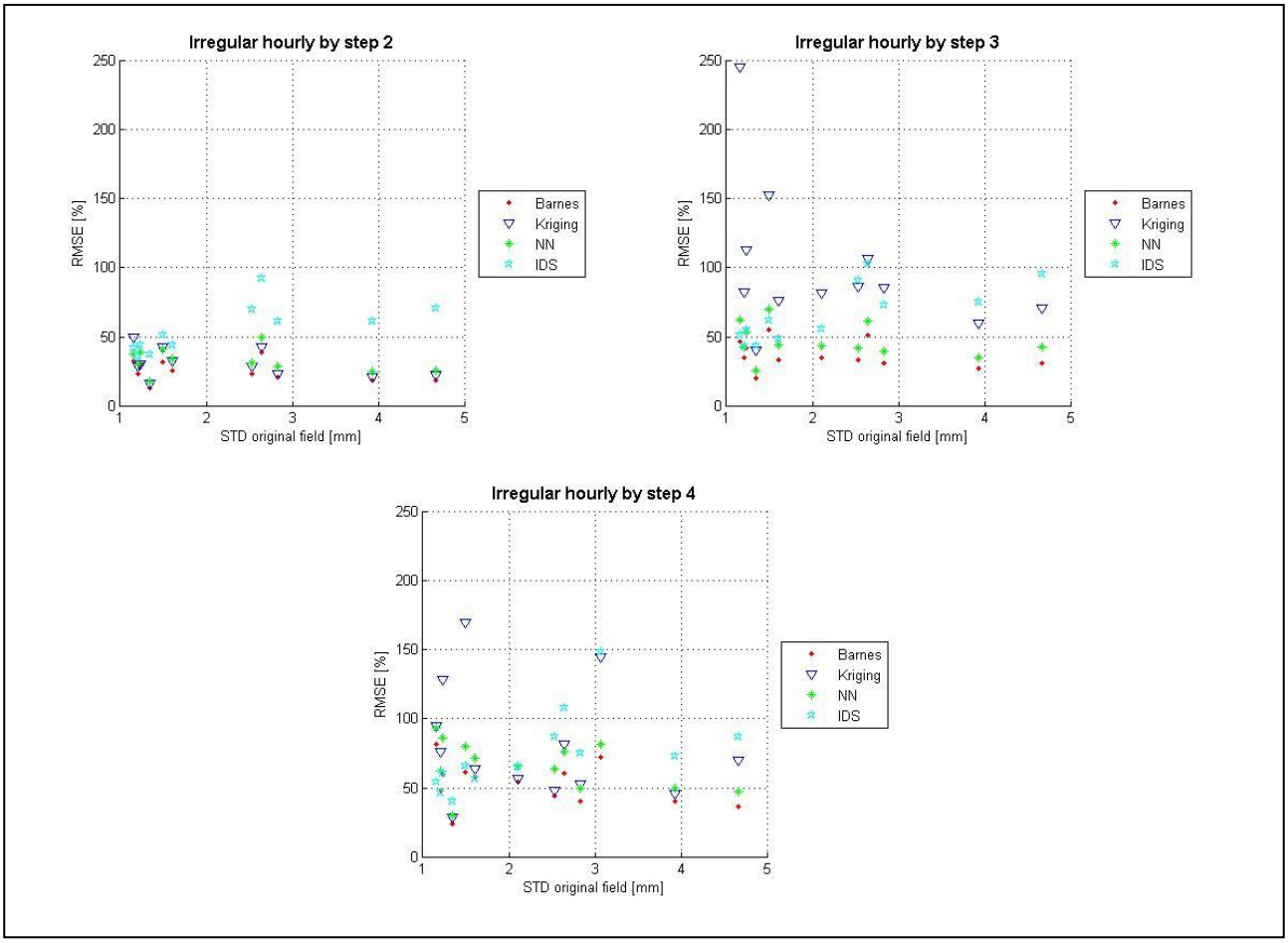

FIG. 2.12 - VS. RMSE% FOR INTERPOLATIONS IRREGULARLY SAMPLED PRECIPITATION DATA.

As shown in Fig. 2.12 the mean RMSE% values computed for hourly precipitation are lower than all previous values computed for istantaneous data. Moreover, RMSE% doesn't show any particular trend with STD of original field.

As last study, two events of November were analyzed sampling up to 11 steps of grid unit as explained above (see page sopra14). The results are follows:

Interpolation	RMSE mean [%]				
	Step 2	Step 3	Step 4	Step 5	Step 6
Barnes	42.23 ± 14.39	58.71 ± 23.24	81.71 ± 39.49	99.15 ± 46.95	102.32 ± 47.02
NN	58.62 ± 21.80	73.40 ± 29.84	97.42 ± 46.12	118.15 ± 52.22	119.58 ± 60.57
IDS	58.72 ± 16.21	85.10 ± 16.11	85.83 ± 18.26	94.74 ± 21.94	94.88 ± 28.09
Interpolation	**Step 7**	**Step 8**	**Step 9**	**Step 10**	**Step 11**
Barnes	140.89 ± 84.16	128.44 ± 69.21	120.49 ± 60.75	136.36 ± 67.11	128.16 ± 69.10
NN	165.41 ± 91.90	147.34 ± 75.69	138.81 ± 68.12	153.33 ± 70.62	145.65 ± 78.82
IDS	94.37 ± 24.64	92.86 ± 22.78	93.98 ± 24.29	97.72 ± 33.73	93.37 ± 25.65

TAB. 2.9 - RMSE MEAN VALUES % OBTAINED BY DIFFERENT INTERPOLATION METHODS AND STEPS FOR HOURLY IRREGULARLY SAMPLED DATA GRID OF NOVEMBER 2010.

The mean STD value of 46 original hourly precipitation fields is less than previous case and it is equal to 1.55 ± 0.79 [mm/h].

In Fig. 2.13 is shown trend of RMSE% mean values with the step for irregular sampling of hourly precipitation mean up to step 11. The mean error values of RMSE% are also indicated with error bars.

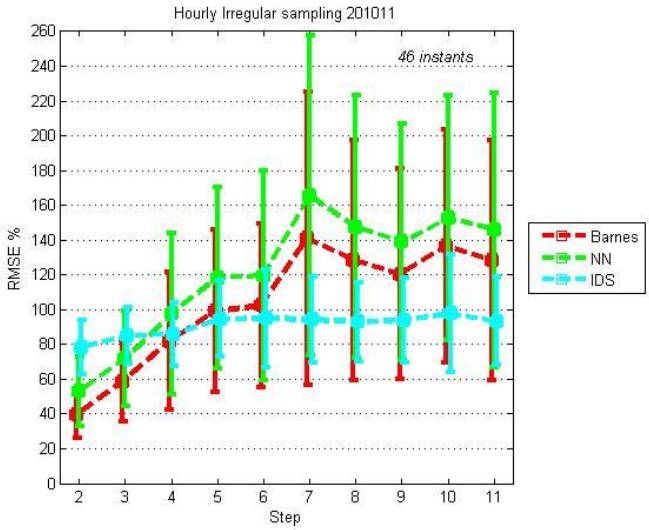

FIG. 2.13 – RMSE% COMPUTED FOR HOURLY IRREGULAR SAMPLING UP TO STEP 11. ERROR BARS ARE ALSO INDICATED.

The trend of RMSE% values is the same for all interpolations: RMSE% increases with the step with values between 42% for Barnes at step 2 and 165% for NN at step 7. The Barnes method has smaller values of RMSE% up to step 3÷4, but for higher steps IDS shows lowest values respect to others methods, with fairly constant values around 92 and 97% and low mean error around 22%.

3 ESTIMATION OF RMSE$_{GROUND}$

Second type of analysis is about instrumental error. RMSE$_{ground}$ is the error due to RG instruments and should be known by owners of the stations. In the final part of the H-SAF Development Phase attempts have been made to evaluate RMSE$_{ground}$. All validation groups (not only for precipitation, but also for soil moisture and snow) have been requested to quote figures to characterise the errors of the best reference ground data that they used. The various validators did this after consultation with the operational units in charge of the observing networks in their institutes. For precipitation the following figures were quoted.

Unit	Ground system	Rain rate	24-h accumulated
UniFerrara	Rain gauge	50 %	25 %
	Radar	100 %	50 %
BfG	Rain gauge	5 ÷ 35 %	5 ÷ 35 %
SHMÚ	Radar	100 % or 15 mm/h (for RR > 10 mm/h)	50 ÷ 100 %
OMSZ	Radar	100 %	50 %
IRM	Rain gauge (interpolated)		70 ÷ 100 %
	Gauge-adjusted radar		50 %
IMWM	Gauge	30 %	
TSMS	Gauge	25 %	10 %
Error range	**Gauge**	**5 ÷ 50 %**	**5 ÷ 100 %**
	Radar	**50 ÷ 150 %**	**50 ÷ 100 %**

TAB. 3.1 - ERRORS OF THE BEST REFERENCE GROUND DATA PROVIDED BY ALL VALIDATION GROUPS.

Tab. 3.1 indicates that the errors due to the ground reference are about 50 – 100 % (of the same order than the H-SAF threshold requirements). It is important to note that the error for instantaneous precipitation is higher than the error for accumulated precipitation and the same applies for radar versus RG data.

Most of the gauges used in the National networks by the Validation Groups are of the tipping bucket type, which is the most common device used worldwide to have continuous, point-like rain rate measurement. Nevertheless, several source of uncertainty in the measurements are well known but difficult to mitigate as: very light rain rates (1 mm h^{-1} and less) can be incorrectly estimated due to the long time it takes the rain to fill the bucket, or underestimation of high rain rates above 50 mm h^{-1} .

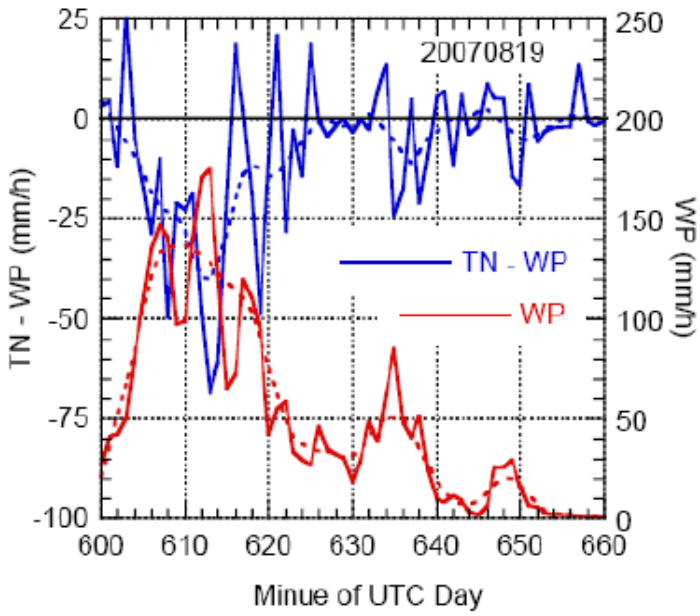

FIG. 3.1 - ONE-MIN RAIN RATE DIFFERENCES TN-WP AND RAIN RATE FROM WP FOR 60-MIN PERIOD. SOLID LINES ARE ONE-MIN OBSERVED VALUES AND DASHED LINES ARE SMOOTH FITS.

Fig. 3.1 shows results of an experiment made by Duchon C. E. and Biddle C. J. (2010) at Norman, in Oklahoma (USA), to investigate about underestimation of tipping-bucket gauges in high rain rates events. WP is a Geonor T-200B weighing-bucket gauge in a pit, TP is a MetOne tipping-bucket gauge in the same pit and TN is identical tipping-bucket gauge to that in the pit located at 105 m. from the pit and it is surrounded by an Alter-type slatted wind screen. This study has analyzed also drifting wind can greatly reduce the size of the effective catching area, if rain does not fall vertically, resulting in a rain rate underestimation when the wind speed at a height of 2m exceeds around 5 m/s (see Fig. 3.2).

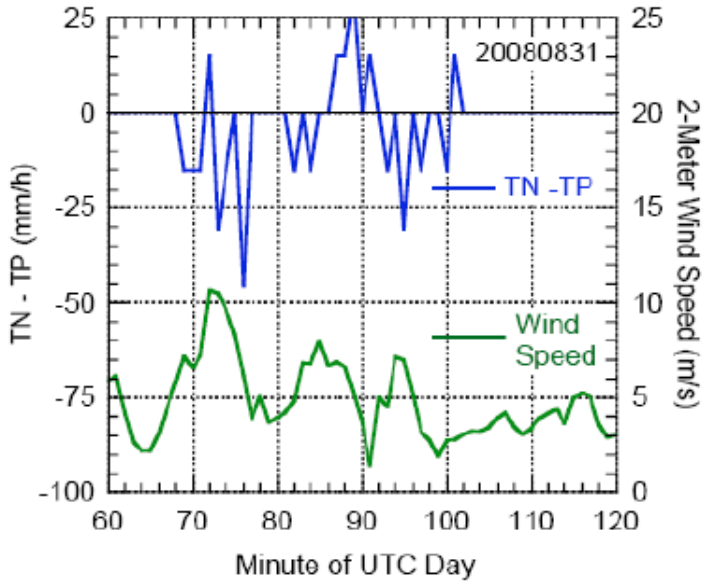

FIG. 3.2 - ONE-MINUTE RAIN RATE DIFFERENCES TN-TP AND 2-M WIND SPEED FOR AN EVENT.

Further errors occur in case of solid precipitation (snow or hail), when the ice particles are collected by the funnel but not measured by the buckets, resulting in a temporal shift of the measurements since the melting (and the measure) can take place several hours (or days, depending on the environmental conditions) after the precipitation event. This error can be mitigated by an heating system that melts the particles as soon as are collected by the funnel. All these errors can be mitigated and reduced, but in general not eliminated, by a careful maintenance of the instrument.

The approach to evaluate the component error of instrument is based on the experiment decided to CIMO to evaluate the performance of several rain gauge instruments. Here the experiment made by Lanza L. G., Vuerich E. and Gnecco I. (2010) to analyze accuracy rain intensity measurement from a field test site is summarized.

3.1 SITE DESCRIPTION

The WMO Field Intercomparison of Rainfall Intensity (RI) Gauges was organized following the request of users and the recommendation of CIMO-XIV. It was conducted from 1 October 2007 to 30 April 2009, in the Centre of Meteorological Experimentations (ReSMA) of the Italian Meteorological Service, in Vigna di Valle, Italy (Fig. 3.3). The Centre is located on the top of a hill at 262 meters above the sea level. It is close to Bracciano Lake and 12 km far from an isolated mountain chain in north direction (600-900 m. above s.l.). The location is generally characterized by a wind regime of dominant flows during the year from SW (warm-humid air masses) and from NE (cold-dry air masses). During precipitation events, an average wind speed of 5 m/s is generally recorded.
The experimental area is a flat 400 m^2 grass field which is equipped with 34 concrete platforms (4 corner-platforms and 30 evenly distributed platforms) and a central 4-fold ISO standard pit for the installation of the set of reference RI gauges. Each platform is supplied with power supply (AC and VDC), serial communication converters, 8 free and 8 coupled high quality double shielded acquisition cables and low voltage threshold discharge protections.

FIG. 3.3 – EXPERIMENTAL AREA OF RESMA – VIGNA DI VALLE, ITALY.

3.2 GAUGES

Participation in the Field Intercomparison of RI was accepted based on requirements. Fifty-four (54) instruments were proposed. The capacity of the field site was limited to 31 rain gauges (including four reference instruments in a pit and four of the same type in the field). All types of rain gauges can fall in two main groups: catching and non-catching types of rainfall intensity measuring instruments. The majority of these instruments were catching type gauges comprising tipping-bucket gauges, weighing gauges and one water level gauge. Non-catching rain gauges were represented by optical and impact disdrometers, one optical/capacitive gauge and one microwave radar gauge.

Catching rain gauges can be characterized as follows:

- They can be calibrated in the laboratory;
- They are able to measure RI within sampling time intervals ranging from a few seconds to several minutes;
- They have finite resolution ranging from 0.001 mm to 1 mm;
- They have reasonably good reproducibility and long-term stability;
- They are widely used in operational practice and are cost effective;
- They are prone to wind-induced catching losses (depending on appropriate wind shielding);
- They are prone to wetting and evaporation losses, especially in low RI.

Regular maintenance, annual calibration and servicing, is needed to obtain high quality measurements.

Non-catching precipitation sensors are mainly used for Present Weather observations including rainfall intensity measurements. Non-catching type rain gauges require low maintenance and very few periodic checks. Therefore, they can be considered particularly suitable for Automatic Weather Stations (AWS) or generally unmanned meteorological stations. Some of them have the advantage to determine the type of precipitation, to distinguish between solid and liquid precipitation, to provide Present Weather information (e.g., METAR and SYNOP codes) and to determine the rain droplets spectra.

FIG. 3.4 – THE WMO FIELD INTERCOMPARISON TEST BED IN VIGNA DI VALLE (ITALY).

3.3 REFERENCE RAIN GAUGE PIT (RRGP)

According to the results of the WMO Laboratory Intercomparison of RI gauges (2004-2005) and the Recommendation 2 of CIMO-XIV (*WMO, 2007a*), corrected tipping bucket rain gauges and weighing gauges with the shortest step response and the lowest uncertainty were used as working reference instruments.
A reference can be defined as a virtual device based on a set of measuring instruments and, according to VIM (the Vocabulary in Metrology), a working reference is a calibrated set of instruments used for controlling/making comparison with measuring instruments.
According to the CIMO Guide (*WMO, 2008a*), the main feature of reference gauge design is to reduce or control the effect of wind on the catch, which is the most serious influence factor for gauges. The use of one single reference instrument in the field intercomparison should be avoided. Gauges are typically mounted at some distance above the ground to reduce debris (dust, needles and leaves) being blown into the orifice. Following Recommendation 2 (CIMO-XIV), four rain gauges were selected as "working reference gauges" and properly installed in four well-drained pits according to the requirements of the ISO/EN-13798:2002 as shown in Fig. 3.5.
The design of the pit took into account dimensions of the gauges and a method of installation of the respective gauge. The sides of the pit are formed of bricks and concrete and they are supported to prevent collapse. As a result, a large pit of 170 cm depth was built and divided in four parts for installing the reference rain gauges. Supporting walls were built around the edges and four galvanized steel grating of 187.5 x 187.5 x 12.0 cm (LxWxH) were rested on pit walls. The base of the pit is deep enough to allow the correct installation of the rain gauge and its levelling. The base of the pit has a recess (extra pit) to allow water to be drained by an electric pumping system.
The grating is strong enough to walk on, to maintain its shape without distortion and it was made in two sections to allow part of it to be lifted, to give access to the rain gauge. The grating was made of galvanised sheet steel. The grating has a central open square for the correct and levelled installation of the rain gauge. To prevent in-splash from the top surface of the grating, the strips of the grating are 0.3 cm thick and the distance between the edge of this central square and the ground is greater than 60 cm.

FIG. 3.5 – THE REALIZATION OF THE REFERENCE RAIN GAUGE PITS AT VIGNA DI VALLE, ITALY (2007).

3.4 INSTRUMENTS CALIBRATION

Prior to installation in the field all reference gauges and the catching type instruments were calibrated in the WMO recognized laboratory at the University of Genoa. Calibration procedures were performed under known and constant flow rates in closely controlled conditions, according to the recommended procedures developed during the WMO

Laboratory Intercomparison of RI Gauges (2004-2005). The laboratory tests were performed at the resolution of one minute. The results of the laboratory calibration, done before the field intercomparison, generally confirm the findings of the Laboratory Intercomparison of RI Gauges.

3.5 REFERENCE VALUE

In the field, all gauges were compared with a RI composite working reference consisting of a set of four reference rain gauges in a standard pit. The RI reference is the best estimation of the 1-minute RI true value that can be obtained from the working reference gauges inside the RRGP, which are two corrected tipping bucket rain gauges (TBRG with correction algorithm) and two weighing gauges (WG) with the shortest step response and the highest accuracy obtained from the WMO Laboratory Intercomparison results (2004-2005).

The determination of a reference value of the rainfall intensity is fundamental for defining the baseline for the intercomparison. Since there are four instruments that were chosen as RI reference gauges, it was necessary to define how to convert their readings into to a RI composite working reference value. The best estimation of a RI composite working reference can be done through the statistical evaluation of the experimental data:

The statistical evaluation of the 1-minute RI reference is made using a ***Weighted Average*** obtained from the rainfall intensities measured by the four references:

$$RI_{ref} = \frac{\sum_i \mu_i RI_i}{\sum_i \mu_i}$$

where μ_i is the weight of the reference rain gauge i and it was calculated taking into account both a global statistical parameter, obtained from the whole data set, and also the evaluation of each single event.

In order to analyze the behaviour of the four reference gauges in the rainfall events, the relative differences (RD) between the measured rainfall intensities and the RI composite working references on 1 minute time scale were computed as follows:

$$RD_i = \frac{RI_i - RI_{ref}}{RI_{ref}} 100\%.$$

In order to compare the gauges to the reference and to assess their agreement with the user uncertainty requirement, a tolerance region was established. For the calculation of the tolerance region we assumed the WMO required measurement uncertainty, of 5% for each rainfall intensity gauge according to CIMO Guide (WMO, 2008°, Part I, Chap. 1, Annex 1.B). So, the tolerance region is composed of this 5% uncertainty and of the uncertainty of the reference ($u_{rel}(RI_{ref})$), thus its value is finally calculated as: $(u_{rel}(RI_{ref})^2 + 5^2)^{1/2}$ (%). The uncertainty of the RI composite working reference in the pit was evaluated to be 4.3 mm/h, leading to a relative uncertainty below 5% above 90 mm/h and higher than the 5% measurement uncertainty required by WMO below 90 mm/h (see Fig. 3.6).

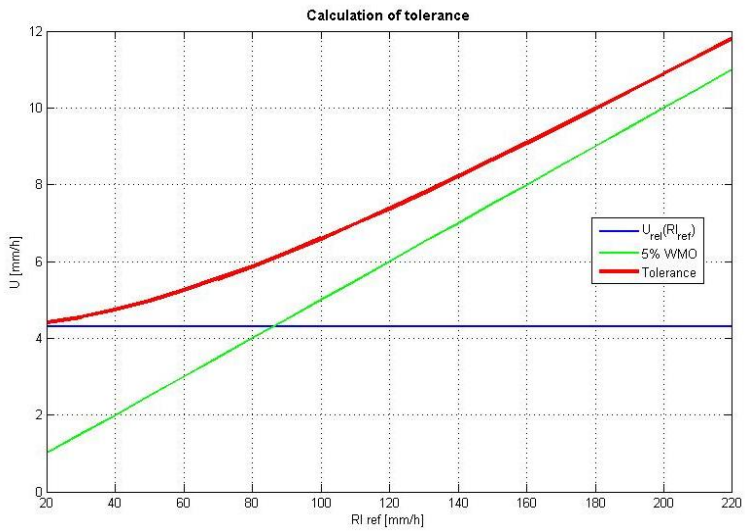

FIG. 3.6 – CALCULATION OF TOLERANCE ERROR FOR RI_{ref}.

In Fig. 3.7, where the relative difference RD between the pit gauges' RI is represented as a function of the reference intensity, it is evident that the dispersion of data is higher for RI below 30 mm/h, where there is also the effect of short and sudden rainfall events.

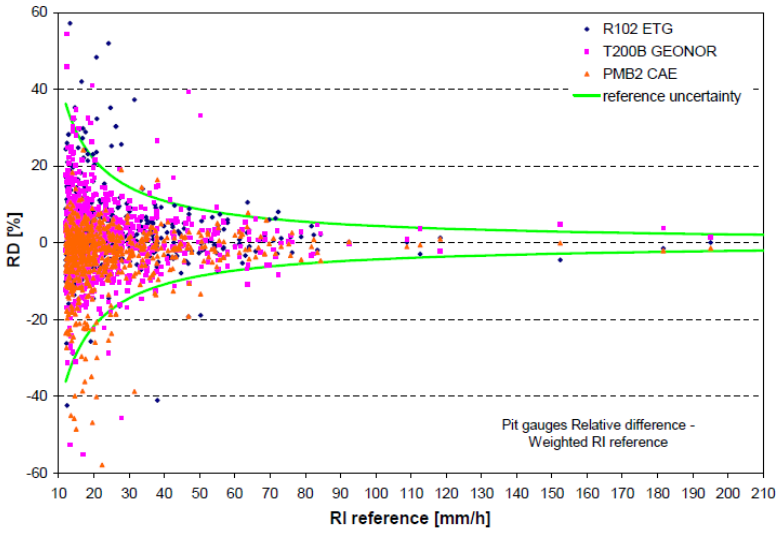

FIG. 3.7 – RI RELATIVE DIFFERENCE: THE WEIGHTS FOR THE RI AVERAGE ARE COMPUTED FROM THE WHOLE DATASET OF EVENTS. GREEN LINES DELIMIT THE REGION WHICH INCLUDES THE 95% OF THE EXPERIMENTAL POINTS.

3.6 QUALITY CONTROL

The Quality Control (QC) procedures have been implemented before the intercomparison so as validated data are provided to the Data Manager and tools for the control of the functioning of instruments are available to the Site Manager.
Quality Control of data is a fundamental component of quality management systems and is important for the examination of data to detect errors and take follow-up actions. The general guidelines are described in the CIMO Guide (WMO, 2008a). The aim of a QC system is to verify the data and to prevent the recurrence of errors. These procedures can

be applied both, in real time and in non-real time as a delayed action for data quality assurance.

3.7 AVAILABLE DATA

The Field Intercomparison has been continuously managed for 18 months in all weather conditions. Excluding three scheduled and one extraordinary maintenance service of data acquisition system and field cabling (totally 23 days), and the periodic maintenance works of rain gauges (documented by the e-logbook). The total availability of 1-minute data was 95.4%, approximately $7.41*10^5$ minute-data of all weather conditions (rain and no rain conditions).
The number of precipitation events (collected in daily files) was 162 (156 events with rain and 6 events with hail and mixed rain/hail).
The following selection criteria were applied to precipitation daily events in order to obtain the best dataset for the purpose of the Field RI Intercomparison:

1. The events used for the analysis were chosen among those that occurred during the period from 13 May 2008 to 30 April 2009. Problems of synchronization and other critical malfunctions where all solved before 13 May 2008. The event of the 30 October 2007 was the only one included (the highest rainfall rate event) that occurred during the period with the problem of synchronization;
2. The events used to retrieve the weights for the calculation of the reference RI had to be characterized by rainfall data with at least 2 consecutive minutes with RI_{1min}>6 mm/h (isolated point/events or those with RI_{1min} < 6 mm/h were discarded).
3. The events used for the RI data analysis had to be characterized by rainfall data with at least 2 consecutive minutes and RI_{1min}>12 mm/h.

According to first criterion, the number of daily events considered for the Field Intercomparison was 85. This was the basis for the "reduced" Field Intercomparison dataset. According to the second criterion, 79 events (out of 85) were used for the calculation of reference RI. According to the third criterion, 43 events (out of 79) were used for the data analysis of all rain gauges. According to the QC daily reports the total availability of valid data was 98.2%. The following table is a summary of available data for the Field Intercomparison.

Total availability of 1-min data (rain/no rain)	***1-min valid data (rain/no rain): percentage of available 1min data that are valid according to QC***	***Total numbers of precipitation daily events***	***Hail and Mixed Rain/Hail events***
T.A. = 95.4%	98.2% of T.A.	162 *(Full FI Dataset)*	6 events
Numbers of synchronized events	***Numbers of events for reference RI calculations***	***Number of events for data analysis of rain gauges***	***Rainfall accumulated over the intercomparison period***
85 *(Reduced FI Dataset)*	79 (28000 1-min data)	43 (740 1-min data)	1325 mm

TAB. 3.2 – SUMMARY OF AVAILABLE DATA.

Tab. 3.3 and the related plot (Fig. 3.8) show the 43 maxima values of reference RI recorded in each event used for data analysis, sorted from higher to lower RI values.

Nr	Date	Max [mm/h]	Nr	Date	Max [mm/h]	Nr	Date	Max [mm/h]	Nr	Date	Max [mm/h]
1	04/11/2008	195.1	12	05/12/2009	69.8	23	31/10/2008	37.5	34	24/01/2009	23.7
2	20/05/2008	152.4	13	22/05/2008	63.5	24	06/12/2009	36.1	35	04/03/2009	23.2
3	28/11/2009	112.7	14	13/05/2008	62.1	25	10/12/2009	34.8	36	20/01/2009	22.2
4	28/10/2008	108.9	15	06/06/2008	61.7	26	29/11/2009	33.6	37	07/02/2009	20.8
5	30/11/2009	107.9	16	01/11/2008	54.9	27	27/04/2009	31.3	38	18/02/2009	17.9
6	23/04/2009	84.4	17	16/12/2009	52.4	28	28/04/2009	29.2	39	10/02/2009	17.4
7	07/01/2009	78.8	18	08/09/2008	47.0	29	24/11/2008	27.8	40	31/03/2009	16.6
8	15/12/2009	75.8	19	01/01/2009	43.9	30	12/11/2008	26.3	41	15/01/2009	13.7
9	15/09/2008	75.4	20	26/01/2009	42.3	31	11/12/2009	26.3	42	14/12/2008	13.6
10	02/03/2009	73.2	21	29/10/2008	39.1	32	01/04/2009	25.8	43	05/03/2009	12.3
11	30/10/2008	72.3	22	27/07/2008	38.3	33	29/03/2009	24.2			

TAB. 3.3 - RI ABSOLUTE MAXIMA RECORDED IN THE DATA ANALYSIS DATASET

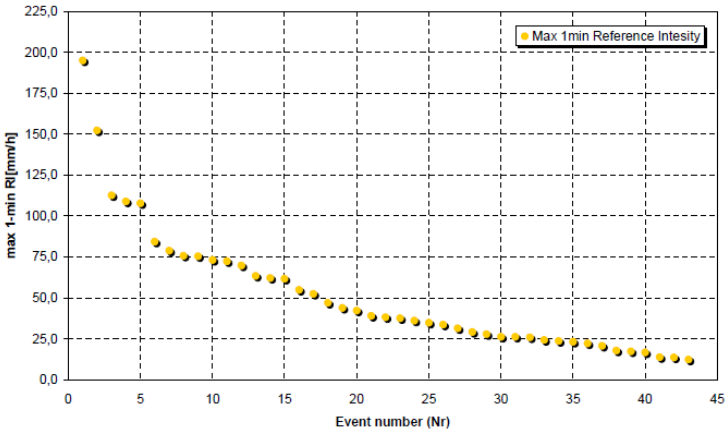

FIG. 3.8 – PLOT OF THE DATA ANALYSIS DATASET

3.8 RESULTS

The plots below (Fig. 3.9) represent the trend of each instrument compared to RI composite working reference, where the trend line is obtained from a power law fitting of the experimental data:

$$RI = a * RI_{ref}^{b}$$

where a and b are constants. The lines of the tolerance region are represented in dashed lines. For easier comparison, the instruments have been grouped according to the measuring principle employed. Also, the data analysis results are separately summarized for the two categories of catching (Fig. 3.9a - Fig. 3.9d) and non-catching type rain gauges (Fig. 3.9e and Fig. 3.9f).

3.8.1 CATCHING TYPE RAIN GAUGES

With regard to tipping bucket rain gauges, the non corrected ones (Fig. 3.9a) tend to understimate precipitation above 40-50 mm/h. The method applied by Software Corrected TBRG (Fig. 3.9b) confirms the possibility to improve the 1-min RI resolution

and to provide accurate field measurements for the whole RI range experienced during the Intercomparison. The method applied by Pulse Corrected TBRG (Fig. 3.9c) revealed the possibility to provide accurate field measurements at higher RI, even if the performance is limited by their resolution at lower RI.

3.8.2 NON CATCHING TYPE RAIN GAUGES

During the intercomparison period, the non-catching type rain gauges needed low maintenance and few periodic checks (especially for the impact disdrometers and the microwave radar), thus this kind of instruments is considered particularly suitable for AWS or generally unmanned meteorological stations. Moreover some of these have the advantage to determine the type of precipitation, to distinguish between solid and liquid precipitation and to provide present weather information (METAR and SYNOP codes).
This field intercomparison has shown the need to improve calibration methods adopted for non catching rain gauges (Fig. 3.9e and Fig. 3.9f) for one-minute RI measurements.

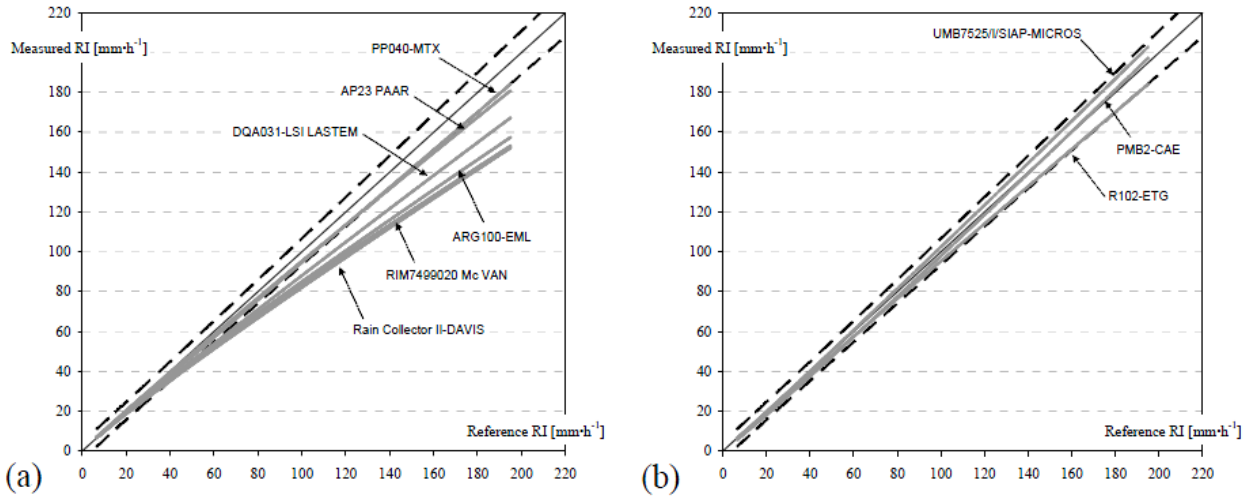

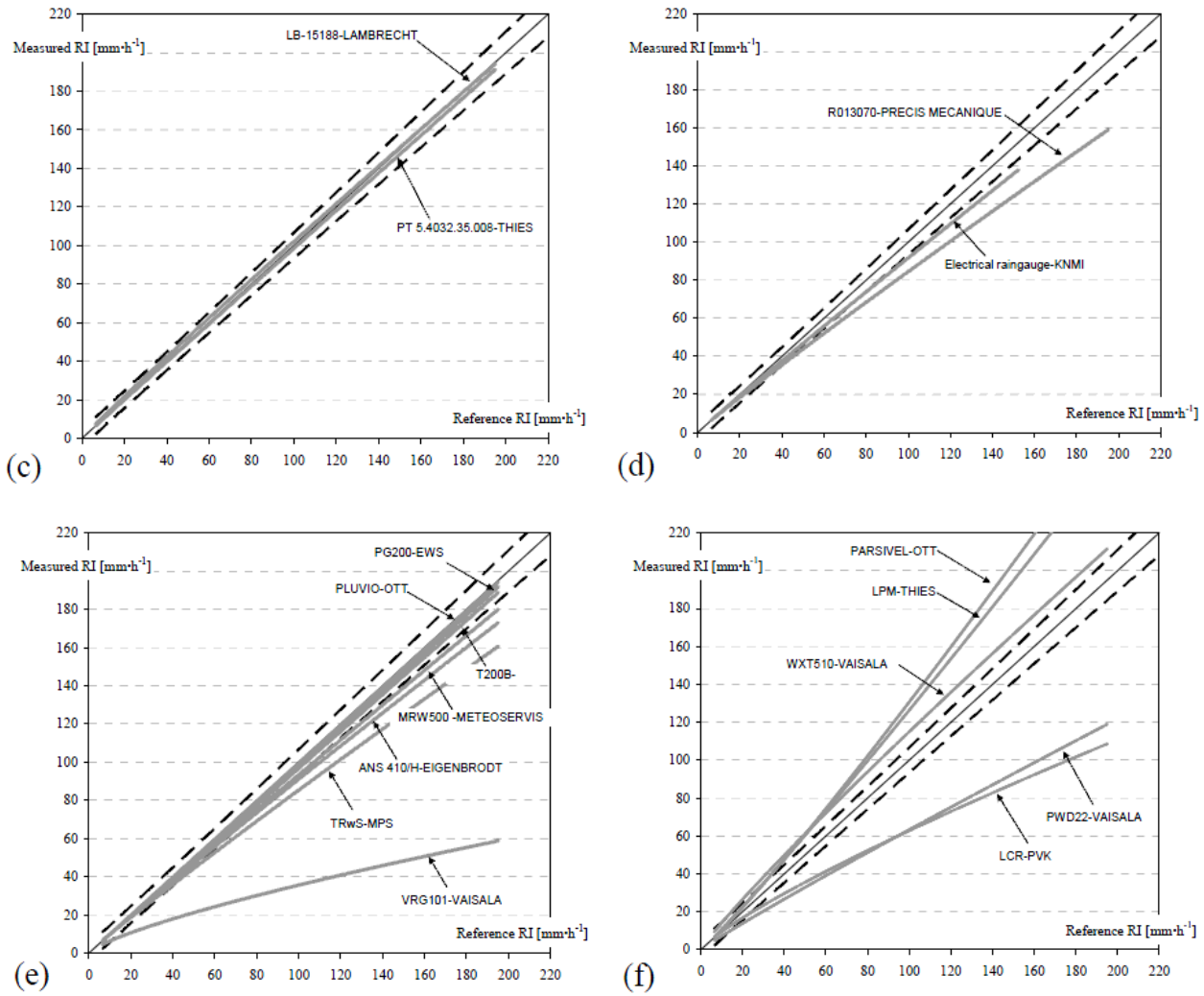

FIG. 3.9 – COMPARISON BETWEEN THE MEASURED AND REFERENCE RAINFALL INTENSITY FOR VARIOUS CLASSES OF RAIN GAUGES: **A)** NON CORRECTED TBRS, **B)** SOFTWARE CORRECTED TBRS, **C)** PULSE CORRECTED TBRS, **D)** MECHANICALLY CORRECTED TBRS OR LEVEL GAUGES, **E)** WEIGHING GAUGES AND **F)** GAUGES BASED ON OTHER MEASURING PRINCIPLES.

In Fig. 3.10 is shown the trend of mean relative percent error for uncorrected TBRG, software corrected TBRG and RI_{ref} relative tolerance. The uncorrected ones tend to underestimate more than corrected ones, especially for precipitation above 40 mm/h. Moreover the uncorrected TBRG show relative error greater than tolerance for precipitation above 50 mm/h. The software corrected TBRG shows a constant mean relative error around 2÷4% for the whole wide range. Correction of TBRG reduces relative error from 14 to only 3% for high rain rate.

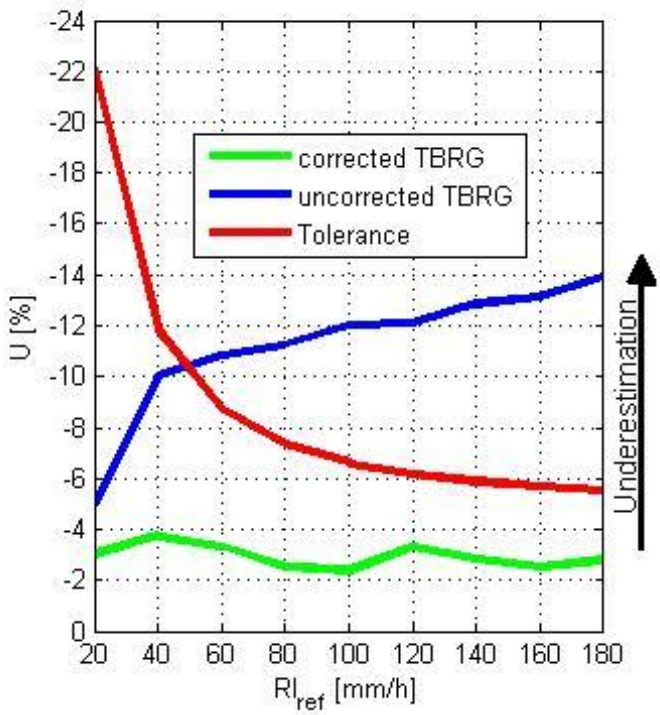

FIG. 3.10 – MEAN RELATIVE PERCENT ERROR OF TBRG SOFTWARE CORRECTED AND UNCORRECTED AND RI_{ref} RELATIVE TOLERANCE.

3.9 CONCLUSIONS

The results confirm that the non corrected TBRG tend to understimate precipitation above 40-50 mm/h. The corrected TBRG performed better than uncorrected ones. The correction could be achieved either by electronically adding an extra pulse or by software based correction. The laboratory and field results confirmed that software correction is the most appropriate method. Very good results with respect to linearity, resolution enhancement and noise reduction could be achieved.

Catching gauges that do not use a funnel are sensitive to external factors, like wind and splash, which could affect the measurements. As a consequence, their noise level is generally increased in comparison to gauges using a funnel.

The best performing weighing gauges and tipping-bucket rain gauges were found to be linear over their measurement range. However, weighing gauges generally cover a wider range.

None of the non-catching rain gauges agreed well with the reference. Disdrometers tended to overestimate the rainfall intensity. Despite their very different calibration procedures, they agreed better to each other than to the reference. This indicated that they had a good degree of precision but were not as accurate as conventional gauges. The microwave radar and the optical/capacitive sensor tended to underestimate the rainfall intensity. For this reason, intercomparison quality control and synchronization procedures were developed to ensure the high quality of the intercomparison data set.

It is recommended that rainfall intensity measurements be further standardized at an international level and based on knowledge obtained from this intercomparison to allow the users to obtain homogeneous and compatible data sets. The procedure adopted for performing calibration tests in the laboratory should become a standard method to be used for assessing the instruments' performance.

4 COMPARISON OF INTERPOLATION METHODS

In this last analysis the behaviour of two interpolation techniques (Barnes and Kriging) most used by VG are been studied as a function of the average minimum distance (AMD) between RG.

4.1 DATA

For this study italian RG data provided by DPC are been used as explained in Tab. 4.1.

Period	January and July 2010
Total RG	~1600
Time resolution	1h
Rainfall resolution	0.2 mm/h
AMD	8.2 Km

TAB. 4.1 – FEATURES OF DATASET USED IN THIS STUDY.

In Fig. 4.1 is shown an hourly instant as example of spatial distribution data.

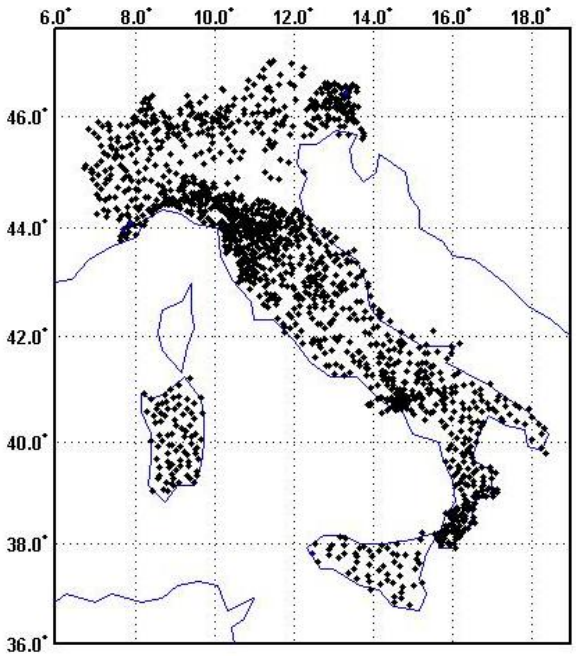

FIG. 4.1 – SPATIAL DISTRIBUTION OF RG IN ITALY.

4.2 METHODOLOGY

To analize interpolation methods trend as a function of AMD is been selected an area (9.0-12.2°E and 43.4-44.8°N) with high-density of RG as represented in Fig. 4.2.

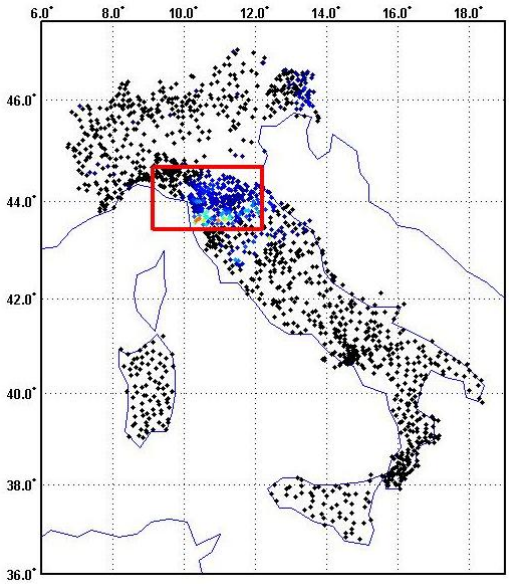

FIG. 4.2 – AREA SELECTED IN THIS STUDY.

In this area there are 340 RG with an AMD = 5.5 Km. The interpolation techniques are been applied to these data to obtain a map of high-resolution 1x1 km as shown below:

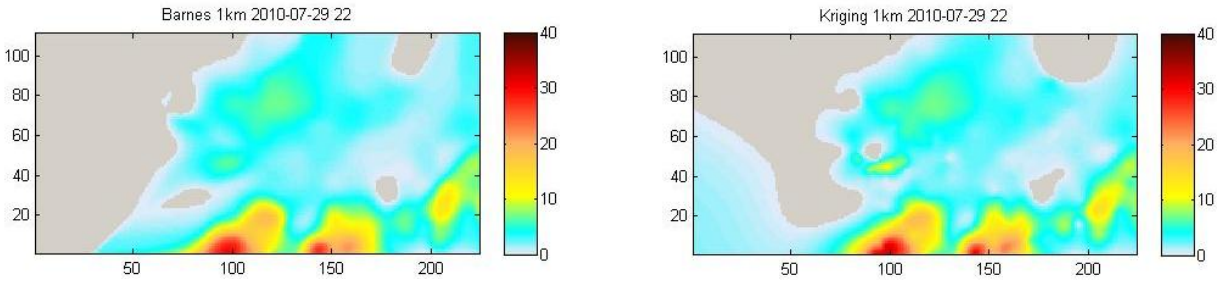

FIG. 4.3 – INTERPOLATIONS: BARNES (ON THE LEFT) AND KRIGING (ON THE RIGTH).

Subsequently, satellite observations of SEVIRI, SSMI/S and AMSU are simulated making an average spatial as a function of correspective IFOV (see Tab. 4.2) obtaining maps as shown (only for Barnes) in Fig. 4.4.

Sensor	**Pixel (Km)**
SEVIRI	4 x 4
SSMI/S	11 x 11
AMSU	20 x 20

TAB. 4.2 – DIMENSION OF PIXEL (1X1 KM) FOR DIFFERENT SATELLITE SENSORS.

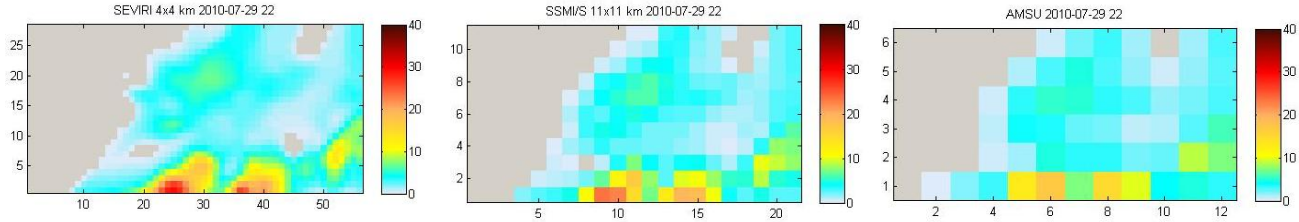

FIG. 4.4 – SIMULATION OF DIFFERENT SATELLITE OBSERVATIONS.

Assuming that values of precipitation obtained at various resolutions (IFOV) with the interpolation of all RG (as explained above) are the best possible, is been calculated some statistical scores to evaluate as the situation changes by varying the AMD (by removing the stations) up to 25 km to simulate the AMD of all countries (see Tab. 2.3 page 14).

To obtain a seasonal statistical measure of the ability of interpolation methods for each month (January and July) the first 20 instants in which the most number of stations had recorded rainfall were analyzed. This to avoid studying cases without precipitation. For each instant statistical scores were computed varying AMD from 7.5 Km to 25 Km by steps of 2.5 Km. Moreover, to increase statistics, each AMD was obtained by 4 runs varying randomly the stations removed.

4.3 RESULTS

The results obtained in this analisys are shown. The statistical scores computed are: RMSE, RMSE%, R^2, POD, FAR, ETS and BIAS. In all graphics SEVIRI is indicated by solid line, SSMI/S by dash-line and AMSU by dot-line. Results obtained with Barnes are shown on the left, Kriging on the rigth. The results for July 2010 are shown below in Tab. 4.3.

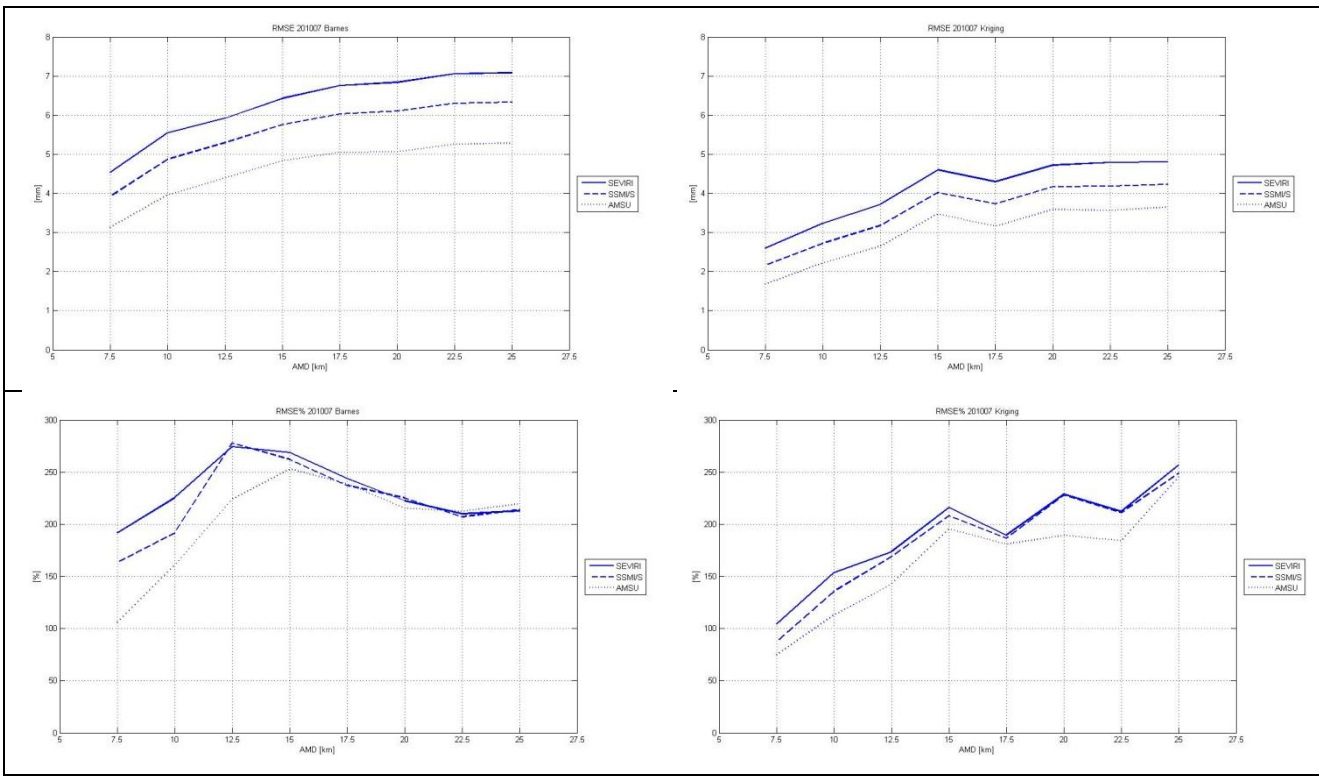

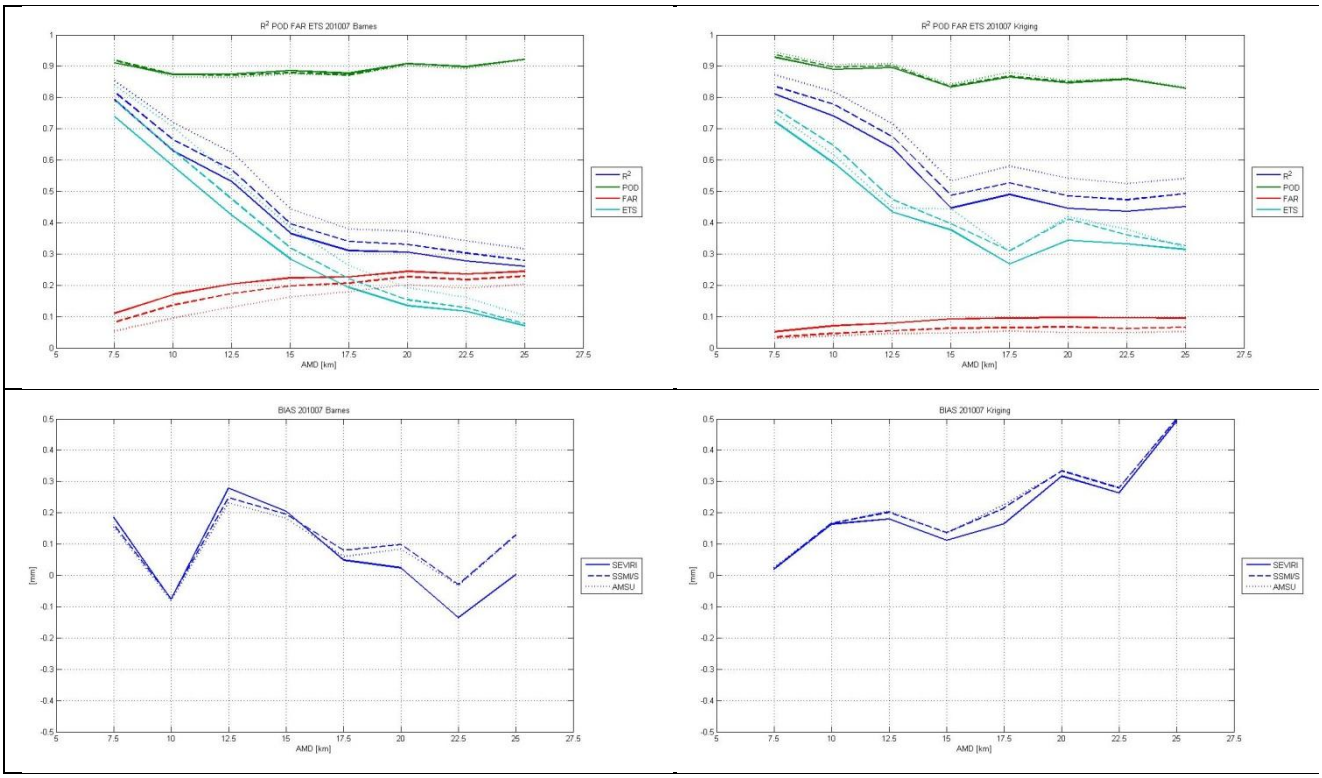

TAB. 4.3 – STATISTICAL SCORES FOR JULY AT DIFFERENT AVERAGE MINIMUM DISTANCES BY BARNES AND KRIGING INTERPOLATION.

Differences between different sensors are negligible. The results are very similar between Barnes and Kriging. In particular, Kriging shows the best results especially for RMSE with a mean value around 3.5 mm (mean value for Barnes is 5.5 mm). About RMSE% Barnes reached a peak of 277% but tends to stabilize at around 220%. Kriging instead has a more linear behavior: the values tend to increase but they are always lower than those obtained with Barnes (except for AMD of 25 Km). POD is similar in both with high-values (~ 0.9), FAR is smaller for Kriging (never more than 0.1). Also R^2 and ETS are better for Kriging. Finally, the BIAS values presented in both methods are very low and always less than 0.5 mm.

Results for January 2010 are represented below in Tab. 4.4.

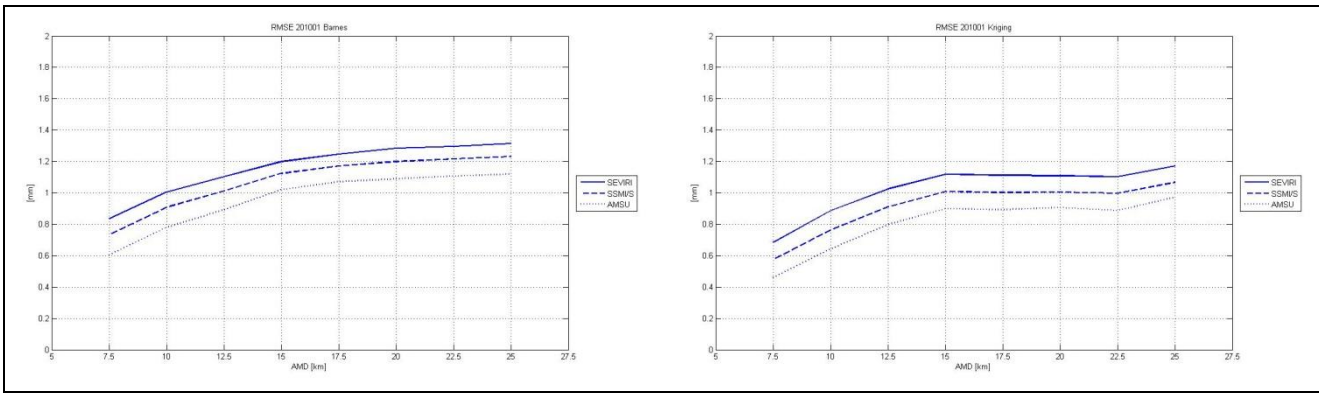

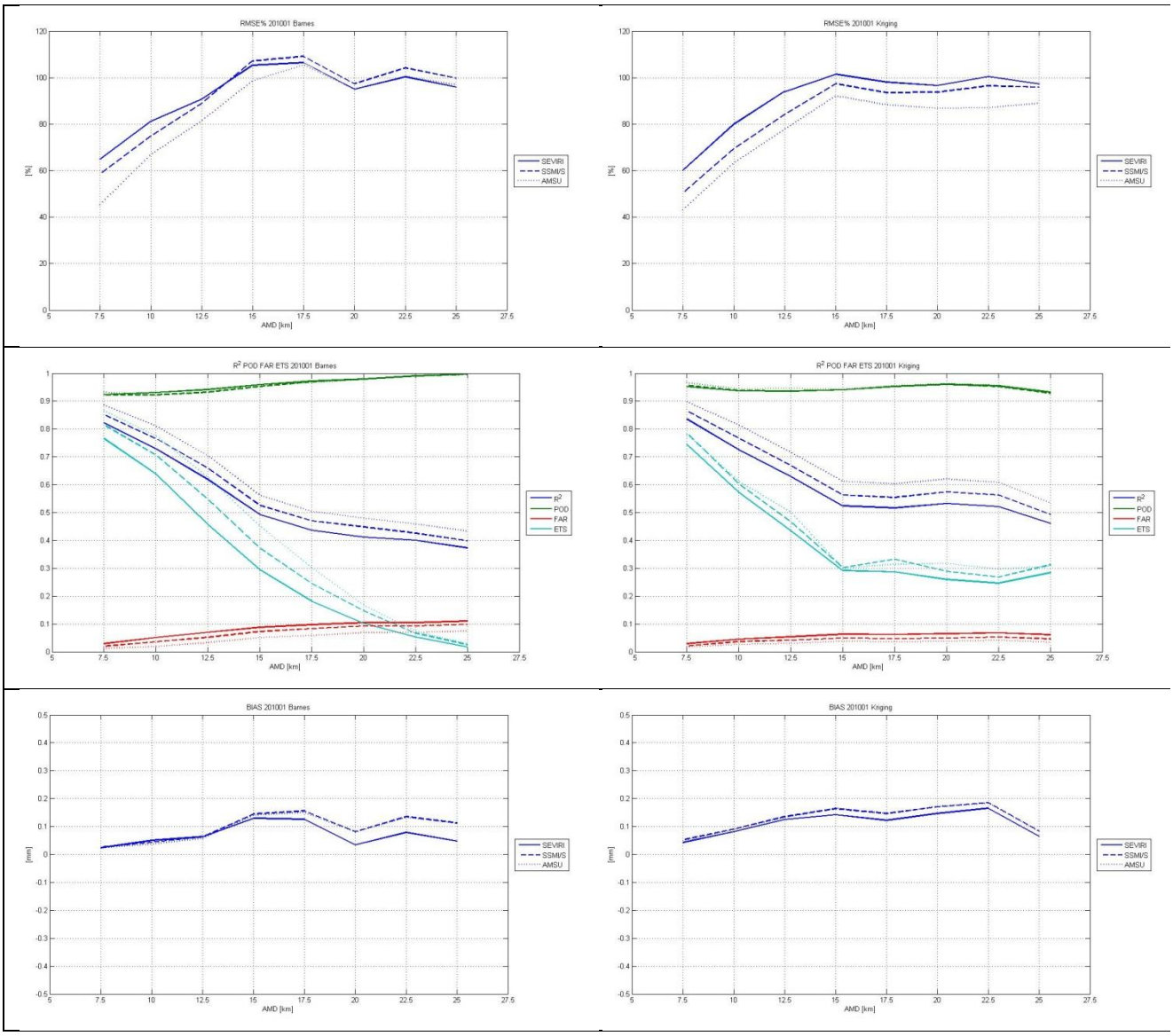

TAB. 4.4 - STATISTICAL SCORES FOR JANUARY AT DIFFERENT AVERAGE MINIMUM DISTANCES BY BARNES AND KRIGING INTERPOLATION.

The results obtained for the month of January are better than those obtained for the month of July due to the prevalence of the phenomena of lower intensity. For example in July RMSE for the Barnes method range from 3 to 7 mm while in the month of January is only 1.3 mm at high AMD. RMSE% decreases even more than 50%, reaching the maximum value of only 110% (previously was 270%). Even R^2 POD and FAR indicate an improvement, as well as BIAS not passes a value of 0.2 mm.

The comparison between Barnes and Kriging highlights the similarity between the two methods, however, the Kriging proves to have better values. The maximum value for RMSE and RMSE% are around 1 and 100% respectively. Even FAR, ETS and R^2 scores indicate a slight improvement compared to Barnes, especially for large AMD. Finally, the BIAS in both cases is very small (always less than 0.2 mm) and as previously is in favor of the Barnes method.

5 CONTINUOUS PRECIPITATION FIELD RETRIEVED FROM GROUND DATA

The lack of information of rain gauge network could be solved with a continuous field retrieved from radar map or from a NWP. In this analysis a prototype of a continuous precipitation field retrived from RG data has been implemented.

5.1 WHY RETRIEVE A PRECIPITATION CONTINUOUS FIELD?

Accurate measurements of precipitation are important not only to weather forecasters and climate scientists, but also to a wide range of decision makers, including hydrologists, agriculturalists, emergency managers, and industrialists. Precipitation measurements provide essential information about the global water cycle and the distribution of the Earth's latent heating, which has direct effects on the planetary circulation of the atmosphere. However, the historical record of precipitation observations is limited mostly to land areas where rain gauges can be deployed, and measurements from those instruments are sparse over large and meteorologically important regions of the earth, such as over the Amazon and equatorial Africa. Furthermore, precipitation observations over the oceans are limited. An important source of global precipitation information is short-range forecasts from NWP model or from radar map that can be used to retrieve a precipitation continuous field. The great advantage of a precipitation continuous field is the global estimates of precipitation providing information on rainfall frequency and intensity in regions that are inaccessible to other observing systems such as rain gauges.

5.2 PRECIPITATION ESTIMATES FROM SATELLITE OBSERVATION AND NUMERICAL MODELS

With the advent of meteorological satellites in the 1970s, scientists developed techniques to estimate precipitation from radiometric observations from satellites, which provide coverage over most of the globe. The first techniques used visible or infrared data to infer precipitation intensity based on the reflectivity of clouds (visible) and from cloud-top temperature (infrared). Both of those types of techniques yield crude estimates of precipitation because the link between cloud properties and precipitation is weak (Ebert et al., 2007). In the 1980s, information became available from passive microwave sensors that were deployed on polar-orbiting spacecraft, which provided more accurate estimates of rainfall than visible or infrared data.

Several studies found that for instantaneous rainfall, algorithms using MW observations gave more accurate estimates than those using IR observations only. As the time scale increased to daily and monthly, the IR and MW-IR algorithms performed comparably or even better than the MW-only algorithms. This was mainly due to the much greater

sampling from the geostationary satellites carrying IR instruments, compared to the limited sampling from microwave instruments on polar orbiting satellites. Furthermore, greater accuracy was shown for tropical, convective, and summertime rainfall, and poorer accuracy for stratiform, mid-latitude, and wintertime rainfall.

Ebert et al. (2003) showed that the models had greatest accuracy for mid-latitude, large-scale, and wintertime rainfall while satellite estimates performing best in summer for tropical and convective rainfall: it is clear that the strengths and weaknesses of satellite estimates and NWP models are complementary.

5.3 DATA

As ground precipitation data the hourly cumulated rain gauges data provided by the Italian DPC (as shown on page 34) are been used. Moreover, a NWP model (COSMO-ME also known as PR-ASS-1) is been considered.

Product PR-ASS-1 (*Instantaneous and accumulated precipitation at ground computed by a NWP model*) is the output of the operational COSMO-ME NWP model in use at CNMCA.

The role of PR-ASS-1 is to provide a background precipitation field regular in space and time, unlike satellite-derived observations that are available at changing times and locations, depending on the specific orbit. The product has been developed, is operationally running and is being progressively improved at CNMCA. It is a “best effort” product: e.g., the covered area (as shown in Fig.), and the number of runs/day will not meet H-SAF requirement by the end of the Development Phase; but it is a fully operational product.
The COSMO-ME model having a 7 km grid spacing uses a cumulus parameterization;
The output consists of five figures at 3-hour intervals:

- ✓ the precipitation rate and
- ✓ the accumulated precipitation over the previous 3, 6, 12 and 24 hours.

FIG. 5.1 shows an example of PR-ASS-1 product, a 24-hour accumulated precipitation map. Map is in *equal latitude/longitude projection*. The product result from the forecasting run started at a T0 conveniently in advance so as to enable the output to be sufficiently stabilised. The accumulated precipitation in figure refers to the previous 24 h.

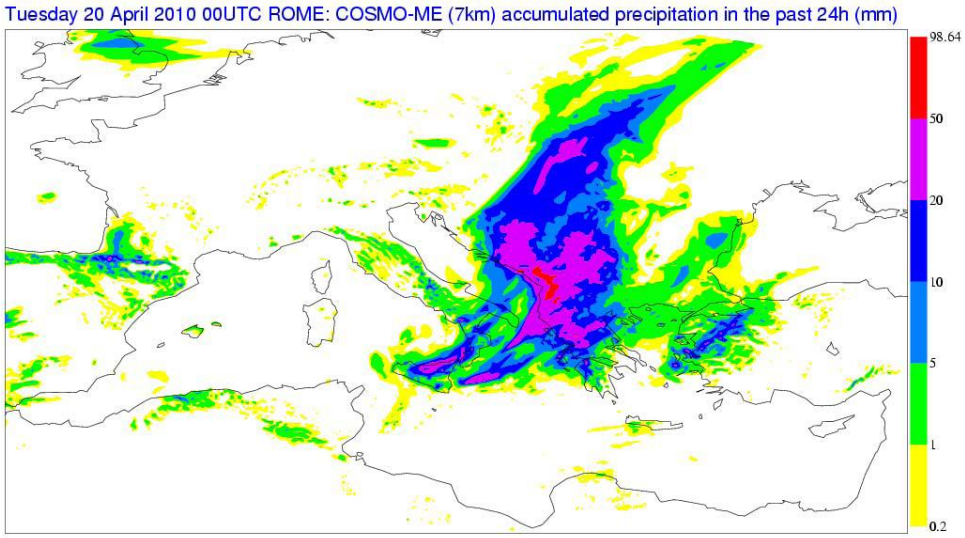

FIG. 5.1 - 24-HOUR ACCUMULATED PRECIPITATION FROM COSMO-ME FOR 20 APR 2010, 00 UTC. FORECAST RUN INITIALISED AT 00 UTC OF 19 APR 2010.

COSMO-ME runs currently two times a day, at 00 and 12 UTC, therefore the observing cycle is $\Delta t = 12\ h$ (to be reduced to Δt = 6 h in the near future, when runs at 06 and 18 UTC will be added). All products are outputted at 3-hour intervals, that therefore represents the sampling time. The timeless for COSMO-ME (that is defined as the time between observation taking and product available at the user site assuming a defined dissemination mean) is currently ~4 h.

5.4 METODOLOGY OF THREE HOURS CUMULATED PRECIPITATION ANALYSIS

To obtain an analysis of cumulated precipitation every 3 hours PR-ASS-1 was considered as first-guess. Three hours cumulated ground precipitation was computed simply summing three successive hourly rain gauges data. Only rain gauges presents in all hours was considered.

Next, the Kriging interpolation applied to three hours cumulated RG data was performed obtaining interpolated data (and relative error in the form of variance s^2) at the NWP model grid.

For every PR-ASS-1 grid point data variance was computed according to values obtained from mean validation results.

An optimal interpolation was performed between PR-ASS-1 and 3h cumulated RG precipitation interpolated data considering variance values for every grid point. The precipitation analysis P was computed by:

$$P_{(i,j)} = a_{1_{(i,j)}} P_{1_{(i,j)}} + a_{2_{(i,j)}} P_{2_{(i,j)}}$$

with $a_{1(i,j)} = \frac{\sigma^2_{2(i,j)}}{\sigma^2_{1(i,j)}+\sigma^2_{2(i,j)}}$ and $a_{2(i,j)} = \frac{\sigma^2_{1(i,j)}}{\sigma^2_{1(i,j)}+\sigma^2_{2(i,j)}}$, where $\sigma^2_{1(i,j)}$ and $\sigma^2_{2(i,j)}$ are variance values computed for PR-ASS-1 (1) and RG (2) data respectively in every (i,j) NWP model grid point.

In this mode RG data will have greater weight on land, i.e. near the same stations, while on sea the resulting precipitation will be mainly derived from NWP model. Near the coast will merge the two data sources in function of the errors relative.

5.5 RESULTS

In Fig. 5.2, on the left the RG data 3h cumulated the 12th December, 2011 at 12:00 UTC is shown. This event is characterized by diffuse and low intensity stratiform precipitation typical of winter rainfall. On the rigth is shown the COSMO-ME output that represents the total 3h cumulate precipitation at ground foreseen for the same interval time.

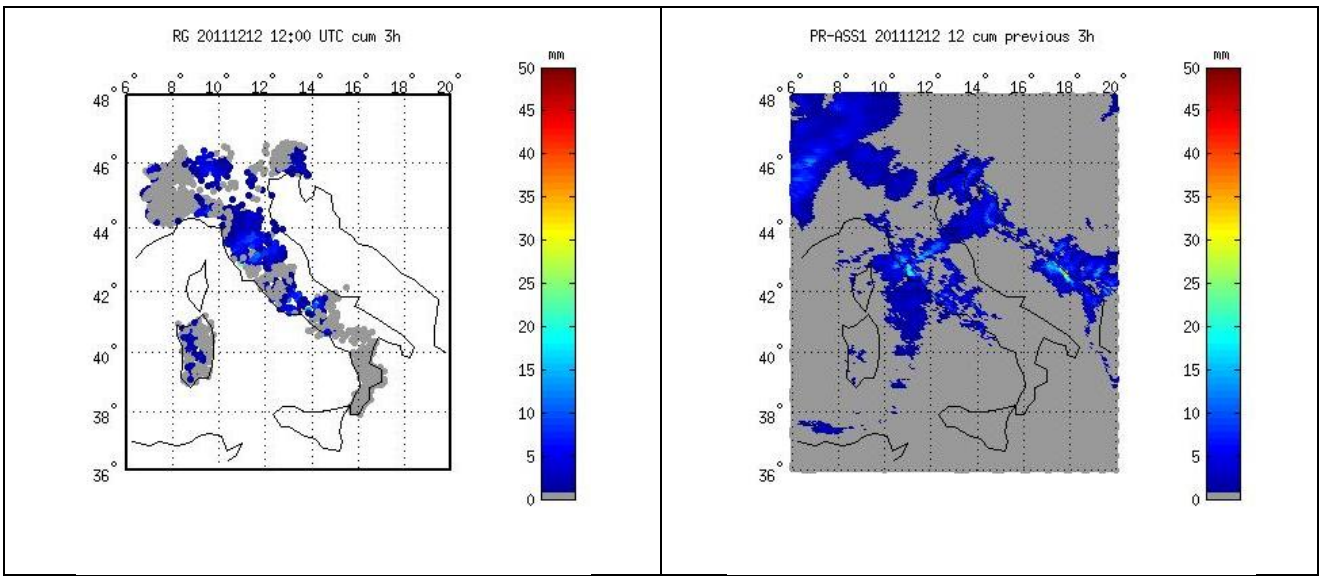

FIG. 5.2 – SOURCES DATA FOR 12 DECEMBER 2011 AT 12 UTC. ON THE LEFT: 3H CUMULATED RG DATA; ON THE RIGTH: PR-ASS-1 3H.

In Fig. 5.3 the precipitation analysis obtained by the optimal interpolation from RG and PR-ASS-1 data is presented.

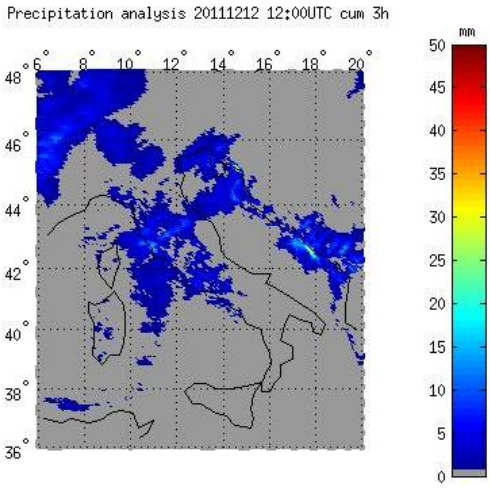

FIG. 5.3 – PRECIPITATION ANALYSIS FOR 3H CUMULATED RAINFALL OF 12 DECEMBER 2011 AT 12 UTC.

The precipitation analysis essentially confirms the model prediction. A small difference is evident on central-north Italy with a more widespread of precipitation with a maximum value slightly less pronounced respect to the prevision.

A second analysis of the 6th November, 2011 at 12:00 UTC (3h accumulate) is shown below. In this case the precipitation is convective type with maximum values over 50 mm/3h. On the right, the PR-ASS-1 model output is shown.

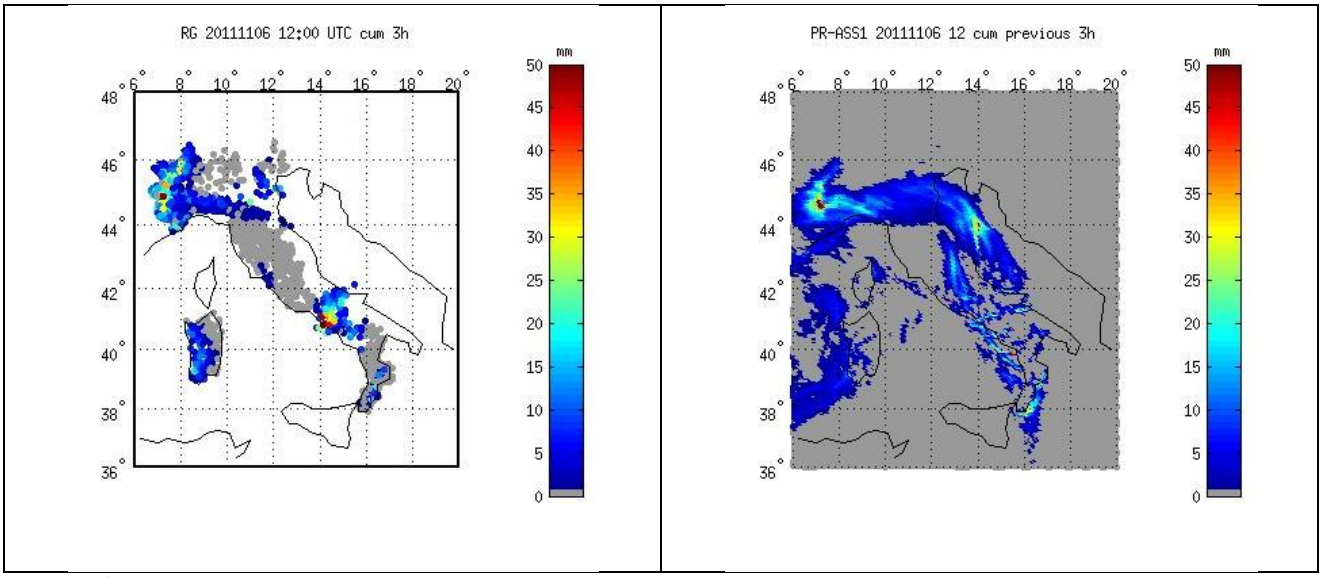

FIG. 5.4 - SOURCES DATA FOR 6 NOVEMBER 2011 AT 12 UTC. ON THE LEFT: 3H CUMULATED RG DATA; ON THE RIGTH: PR-ASS-1 3H.

The precipitation analysis obtained is presented in Fig. 5.5.

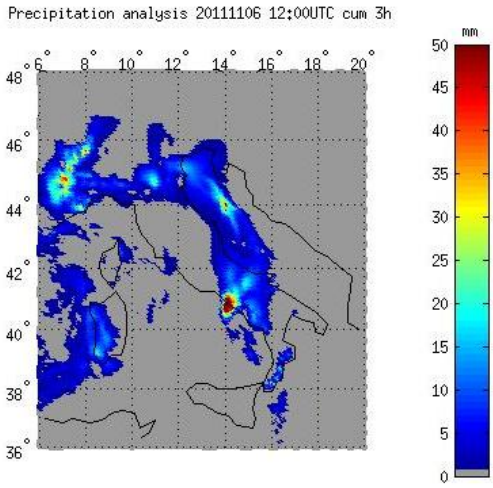

FIG. 5.5 - PRECIPITATION ANALYSIS FOR 3H CUMULATED RAINFALL OF 6 NOVEMBER 2011 AT 12 UTC.

The analysis shows precipitation pattern and values very similar to the forecast model. However several differences are evident in particular on central-south Italy where the precipitation are been more intense and widespread than forecast.

6 CONCLUSIONS

In the H-SAF context instantaneous and accumulated precipitation have been usually evaluated respect to radar and rain gauge data. Radar and rain gauge derived fields have been assumed as the "truth" and no error has been considered. The experience and the literature show that this assumption is not correct (Graves, Valdès, Shen and North (1993), Llasat, Rigo, Ceperuelo and Barrera (2005), Lanza, Vuerich and Gnecco (2010)). This study has wanted clarify about the error structure of precipitation field retrieved from rain gauges evaluating the limits of accuracy requirements proposed during the Development Phase.

The HSAF Validation Group calculated the error in rainfall estimation from satellite considering as reference rain measured by rain gauges at ground. The result of this validation activity indicates the difference between the satellite and the ground measurement; it is the Root Mean Square Difference of satellite vs. reference that depends on $RMSE_{sat}$, $RMSE_{ground}$ and $RMSE_{comparison}$. The first is the error due to satellite rainfall estimation that should be final result of the validation activity; $RMSE_{ground}$ is the error due to the RG at ground and $RMSE_{comparison}$ is mainly due to the upscaling/downscaling and interpolation process.

With regard to $RMSE_{comparison}$ is shown that the for all methods RMSE increases with distance of interpolating data and doesn't show a strong dependence by standard deviation of interpolating field. It was computed that RMSE is higher (up to twice) for instantaneous rain than for hourly precipitation data because high temporal-spatial variability of precipitation. The best values of RMSE% are been computed for the Barnes method up to step 4 (with values around 40÷80%), but for higher steps the Inverse Distance Squared method shows lowest values of RMSE% (around 94%) and respective mean error (around 22%) for hourly precipitation data irregularly sampled.

The comparison between Barnes and Kriging applied to RG data at different spatial density shown as both methods are similar but, in general, Kriging proves to have better results specially in terms of RMSE and RMSE%. Moreover, seasonal comparison shows that errors are lower in winter than in the summer months due to phenomena of lower intensity and inhomogeneity in January.

With regard to $RMSE_{ground}$, analysis confirm that corrected tipping-bucket rain gauges performed better than uncorrected ones with errors that decrease, in some cases, from 20% to only 3% for high rain rate. Most of the gauges used in the National networks by the Validation Groups are of the tipping bucket type, which is the most common device used worldwide to have continuous, point-like rain rate measurement. Nevertheless, several source of uncertainty in the measurements are well known but difficult to mitigate. First, very light rain rates (1 mm h^{-1} and less) can be incorrectly estimated due to the long time it takes the rain to fill the bucket. On the other side, high rain rates

(above 40÷50 mm h^{-1}) are usually underestimated due to the loss of water during the tips of the buckets.
Further errors occur in case of solid precipitation, when the ice particles are collected by the funnel but not measured by the buckets, resulting in a temporal shift of the measurements since the melting (and the measure) can take place several hours (or days, depending on the environmental conditions) after the precipitation event. This error can be mitigated by an heating system that melts the particles as soon as are collected by the funnel. All these errors can be reduced, but in general not eliminated, by a careful maintenance of the instrument.

Catching gauges that do not use a funnel are sensitive to external factors, like wind and splash, which could affect the measurements. As a consequence, their noise level is generally increased in comparison to gauges using a funnel. Drifting wind can also greatly reduce the size of the effective catching area, if rain does not fall vertically, resulting in a rain rate underestimation. However, it was observed that error is negligible for wind speeds below 5 m/s.

The best performing weighing gauges and tipping-bucket rain gauges were found to be linear over their measurement range. However, weighing gauges generally cover a wider range. None of the non-catching rain gauges agreed well with the reference.

BIBLIOGRAPHY

Barnes, S. L. (1964). A technique for maximizing details in numerical weather map analysis. *Journal of applied meteorology , 3*, 396-409.

Barnes, S. L. (1994). Application of the Barnes objective analysis scheme. Part I: Effect of undersampling, wave position, and station randomness. *Journal of Atmospheric and Oceanic Technologic , 11* (6), 1433-1448.

Barnes, S. L. (1994). Application of the Barnes objective analysis scheme. Part II: Improving derivate estimates. *Journal of Atmospheric and Oceanic Technology , 11* (6), 1449-1458.

Barnes, S. L. (1994). Applications of the Barnes objective analysis scheme. PArt III: Tuning for minimum error. *Journal of Atmospheric and Oceanic Technology , 11* (6), 1459-1469.

Duchon, C. E. (2010). Undercatch of tipping-bucket gauges in high rain rate events. *Advances in Geosciences* , 11-15.

Goodison, B. E., Louie, P., & D., Y. (1998). WMO Solid orecipitation mesurement intercomparison. *WMO/TD - No. 872* , 318.

Graves, C. E., Valdès, J. B., Shen, S. S., & North, G. R. (1993). Evaluation of sampling errors of precipitation from spaceborne and ground sensors. *Journal of Applied Meteorology* , 374-385.

Koch, S. E., Desjardins, M., & Kocin, P. J. (1983). An interactive Barnes objective map analysis scheme for use with satellite and conventional data. *Journal of Climate and applied Meteorology , 22* (9), 1487-1503.

Lanza, L. G., Vuerich, E., & Gnecco, I. (2010). Analysis of higly accurate rain intensity measurements from a field test site. *Advances in Geosciences* , 37-44.

Lanza, L., Leroy, M., Alexandropoulos, C., Stagi, L., & W., W. (2005). *WMO laboratory intercomparison of rainfall intensity gauges.*

Llasat, M. C., Rigo, T., Ceperuelo, M., & Barrera, A. (2005). Estimation of convective precipitation: the meteorological radar versus an automatic rain gauge network. *Advances in Geosciences* , 103-109.

Marcotte, D. (1991). Cokriging with Matlab. *Computers & Geosciences* , 1265-1280.

Sauvageot, H., Mesnard, F., & Tenorio, R. S. (1999). The relation between the area-average rain rate and the rain cell size distribution parameters. *American Meteorological Society , 56*, 57-70.

Venugopal, V., Foufola-Georgiou, E., & Sapozhnikov, V. (1999). Evidence of dynamic scaling in space-tima rainfall. *Journal of Geophysical Research , 104* (D24), 31,599-31,610.

Vuerich, E., Monesi, C., Lanza, L. G., Stag, L., & Lanzinger, E. (2009). WMO Field intercomparison of rainfall intensity gauges. *World Meteorological Organisation - Instruments and Observing Methods Rep. No. 99, WMO/TD No. 1504* , 286.

Zeng, X. (1999). The relationship among precipitation, cloud-top temperature and precipitable water over the tropics. *American Meteorological Society , 12*, 2503-2514.